Title: Integrating genetic regulation and single-cell expression with GWAS prioritizes causal genes and cell types for glaucoma

Authors:

Andrew R. Hamel[1,2,3], John M. Rouhana[1,2,3,*], Wenjun Yan[4,*], Aboozar Monovarfeshani[4,*], Xinyi Jiang[5,6], Qingnan Liang[7], Puja A. Mehta[1,2,3], Jiali Wang[1,2,3], Arushi Shrivastava[1,2], Katherine Duchinski[1,2,3], Tavé van Zyl[4,8], International Glaucoma Genetics Consortium (IGGC), Rui Chen[7], Veronique Vitart[5], Joshua R. Sanes[4], Janey L. Wiggs[1,2,3], Ayellet V. Segrè[1,2,3,#]

Affiliations:

[1]Ocular Genomics Institute, Department of Ophthalmology, Massachusetts Eye and Ear, Boston, MA

[2]Department of Ophthalmology, Harvard Medical School, Boston, MA

[3]Broad Institute of Harvard and MIT, Cambridge, MA.

[4]Department of Molecular and Cellular Biology and Center for Brain Science, Harvard University, Cambridge, MA, USA

[5]MRC Human Genetics Unit, Institute of Genetics and Cancer, The University of Edinburgh, Edinburgh, UK

[6]Centre for Genomic and Experimental Medicine, Institute of Genetics and Molecular Medicine, The University of Edinburgh, Edinburgh, UK

[7]Department of Molecular and Human Genetics, Baylor College of Medicine, TX

[8]Department of Ophthalmology and Visual Sciences, Yale School of Medicine, New Haven, CT

* Co-second authors, these authors contributed equally

[#] Correspondence to be addressed to Ayellet V. Segrè: ayellet_segre@meei.harvard.edu

Abstract

Primary open-angle glaucoma (POAG), characterized by retinal ganglion cell death, is a leading cause of irreversible blindness worldwide; however the molecular and cellular causes are not well understood. Elevated intraocular pressure (IOP) is a major risk factor, but many patients have normal IOP. Colocalization analysis of >130 POAG and 112 IOP GWAS loci and overlapping expression and splicing quantitative trait loci (e/sQTLs) in 49 GTEx tissues and retina proposed causal genes for 60% of the loci, that were enriched in extracellular matrix organization, cell adhesion, and vascular development. Analyzing single-nucleus RNA-seq of glaucoma-relevant eye tissues, we found that the colocalizing genes were enriched in known and less well-characterized cell types, including fibroblasts in the conventional and unconventional aqueous outflow pathways; vascular cells in the anterior segment; astrocytes and Müller glia in retina and optic nerve head (ONH); and smooth muscle and vascular endothelial cells in ONH. This study nominated IOP-dependent and independent regulatory mechanisms, genes, and cell types that may underlie POAG pathogenesis.

Introduction

Primary open-angle glaucoma (POAG) is the second leading cause of irreversible blindness worldwide among people over the age of 55[1]. It is characterized by progressive optic neuropathy, caused by gradual death of retinal ganglion cells (RGCs) that transmit visual information from photoreceptors in the retina to the brain via the optic nerve[2]. Elevated intraocular pressure (IOP) is a major risk factor for POAG[3] and is primarily caused by decreased outflow of the aqueous humor, the clear fluid that fills the space in the front of the eye between the lens and cornea. Decreased outflow may be due to abnormal function of structures in the anterior segment of the eye, consisting of the trabecular meshwork (TM)[4] and Schlemm's canal (SC)[5] in the conventional outflow pathway, and the ciliary muscle and iris in the uveoscleral (unconventional) pathway[6]. However, about a third of patients with POAG display optic nerve degeneration in the absence of abnormally high IOP measurements (normal tension glaucoma (NTG))[7], and many people with elevated IOP do not develop glaucoma, suggesting that IOP-independent processes, such as increased RGC susceptibility, even in the normal IOP range, might also lead to optic nerve damage. Currently, neuroprotective therapies are lacking, and medications that reduce IOP have limited effectiveness[2].

68 Gaining a better understanding of the molecular and cellular causes of the disease in the front and
69 back of the eye could help propose novel avenues of therapy.

70 A recent multi-ethnic genome-wide association study (GWAS) meta-analysis of 34,179
71 POAG cases and 349,321 controls of European, Asian, and African ancestries identified 127 risk
72 loci associated with POAG, explaining ~9% of POAG heritability, and a meta-analysis of the
73 European subset identified 68 loci, some of which were not found in the cross-ancestry meta-
74 analysis[8]. A GWAS meta-analysis of IOP performed on 139,555 individuals, primarily of European
75 descendant[9], has identified 133 independent associations in 112 loci, largely overlapping with two
76 other studies[10,11]. The IOP variants' effect sizes and direction of effect are highly correlated with
77 their effect on POAG risk[8,9], and together they explain 9-17% of IOP heritability. Vertical-cup-to-
78 disc ratio (VCDR), central corneal thickness, and corneal hysteresis, a measure of the viscoelastic
79 damping of the cornea, have also been associated with POAG; large GWAS meta-analyses have
80 uncovered 70-200 genetic associations for these traits[12–23].

81 Identifying the causal genes and cell types underlying the genetic associations with POAG
82 and its related traits is challenging; as with other complex traits, the majority of associated variants
83 lie in noncoding regions and due to linkage disequilibrium (LD), they often tag multiple variants and
84 genes, making it difficult to pinpoint the implicated causal gene(s) from sequence alone.
85 Furthermore, genetic regulatory effects in relevant ocular tissues are limited and have not yet been
86 measured at cellular resolution in the eye. However, using single cell or single nucleus RNA-
87 sequencing, human cell atlases and cellular level transcriptomes have been created for several
88 non-diseased POAG-relevant eye tissues, including retina[24,25], the aqueous humor outflow
89 pathway[26,27], and six tissues in the anterior chamber[28].

90 The Genotype-Tissue Expression (GTEx) Project has identified expression quantitative trait
91 loci (eQTLs) and splicing QTLs (sQTLs) in 49 (non-ocular) tissues[29], which have been found to be
92 enriched for genetic associations in relevant tissues with a range of complex diseases and traits[29–
93 31]. eQTLs were recently identified in human peripheral retina[32,33] that contain RGCs. Since many
94 of the GTEx tissues contain cell types that could serve as proxies for the pathogenicity of glaucoma
95 (e.g., neuronal cells in brain as a proxy for RGCs or endothelial cells in artery as a proxy for
96 Schlemm's canal), and e/sQTLs are largely shared across tissues[29], we postulate that e/sQTLs in
97 GTEx tissues could help uncover causal mechanisms and genes underlying at least part of the
98 genetic associations with glaucoma.

99 In this study, we combined e/sQTLs, single-cell expression data from the glaucoma-relevant
100 eye tissues and pathway information with POAG and IOP genetic associations to identify a high
101 confidence set of genes, pathways, and cell types that may play an important role in POAG etiology.

102 We applied two Bayesian-based colocalization methods, eCAVIAR[34] and *enloc*[35] that test whether
103 co-occurring GWAS and e/sQTL signals are tagging the same causal variant/s to all known POAG
104 and IOP GWAS loci and all intersecting e/sQTLs from 49 GTEx tissues and retina. This identified
105 potential causal genes and the e/sQTL direction of effect on POAG risk and IOP levels for ~60%
106 of the loci. These genes were enriched in both previously proposed and new biological processes
107 that may influence POAG risk. To identify key ocular cell types for POAG pathogenesis, through
108 which the proposed POAG or IOP genes may be exerting their causal effect, we extended a method
109 we recently developed, called ECLIPSER (Enrichment of Causal Loci and Identification of
110 Pathogenic cells in Single Cell Expression and Regulation data)[36,37], to e/sQTL-colocalizing genes.
111 ECLIPSER tests whether genes mapped to GWAS loci of a given complex disease or trait are
112 enriched for cell type-specific expression in single cell RNA-seq data of a given tissue, compared
113 to thousands of GWAS loci of unrelated traits. Applying this approach to POAG and IOP e/sQTL-
114 colocalizing genes and single-nucleus expression data of the anterior segment, retina, and optic
115 nerve head, we identified known and less well-established pathogenic cell types for POAG, which
116 suggested both IOP-dependent and neuroprotective pathways. Finally, we tested whether POAG
117 and IOP associations beyond genome-wide significance were enriched among e/sQTLs in GTEx
118 tissues and in retina, and estimated the number of trait associations likely to have a regulatory
119 effect on the traits using an empirical q-value approach. We found significant enrichment in multiple
120 tissues, which suggested over a thousand new genetic regulatory effects on POAG and IOP.
121
122 **Results**
123
124 **Overview of approach and methods.** We applied the following analytical steps to known GWAS
125 loci and genome-wide association summary statistics of POAG and its major risk factor, elevated
126 IOP, to identify genes, regulatory mechanisms, pathways, and cell types that significantly affect
127 POAG risk. First, to propose putative causal genes that may underlie genome-wide significant
128 POAG and IOP GWAS loci, we applied two colocalization methods, eCAVIAR[34] and *enloc*[35], to
129 each GWAS locus and all overlapping *cis*-eQTLs and *cis*-sQTLs in 49 GTEx tissues (release v8[29])
130 and *cis*-eQTLs in peripheral retina[32] (Fig. 1a and Methods). These Bayesian-based methods
131 assess the probability that overlapping GWAS and e/sQTL signals are tagging the same causal
132 variant/s, accounting for local LD and allelic heterogeneity, using slightly different fine-mapping and
133 colocalization approaches (Methods). Second, to identify biological or physiological processes that
134 may be enriched for the proposed causal genes, we applied gene set enrichment analysis to all
135 POAG and IOP colocalizing genes and known signaling and metabolic pathways, gene ontologies,

136 and mouse phenotype ontologies, using *GeneEnrich*[30] (Fig. 1b and Methods). Next, to identify key
137 pathogenic cell types through which the colocalizing genes may be mediating their effect on POAG
138 and IOP, we extended a method we recently developed, ECLIPSER[36,37] to the GWAS-e/sQTL
139 colocalizing genes (Fig. 1c and Methods). ECLIPSER tests whether the expression of genes
140 mapped to GWAS loci is enriched in specific cell types compared to a null distribution of GWAS
141 loci associated with thousands of traits unrelated to ocular diseases which were compiled from
142 Open Targets Genetics (Methods). Briefly, for each trait, tissue, and cell type combination, each
143 POAG or IOP GWAS locus was scored as the fraction of cell type-specific genes mapped to the
144 locus based on e/sQTL colocalization analysis (Methods). Genes were mapped to the null set of
145 GWAS loci based on LD between the GTEx or retina e/sQTLs and the lead GWAS variants, and
146 the loci were similarly scored for cell type specificity. Cell type-specific enrichment of the GWAS
147 locus sets of POAG, IOP and additional related traits was assessed against an LD-independent
148 null distribution, using a Bayesian Fisher's exact test. Genes mapped to the GWAS loci driving the
149 enrichment signal in a specific cell type were proposed to influence the given trait in the
150 corresponding cell type. We applied this method to several ocular tissues relevant to the
151 pathogenesis of glaucoma: six tissues from the anterior segment, including the outflow pathway
152 and ciliary body, retina, and optic nerve head. We found significant enrichment of POAG and IOP
153 genes in specific cell types in both the front and back of the eye that were tested for enrichment in
154 biological pathways compared to a background of genes expressed in a matching GTEx or retina
155 tissue (Methods). Finally, we used *QTLEnrich*[30] to test whether POAG and IOP genetic
156 associations, beyond genome-wide significance, were enriched among eQTLs and sQTLs in GTEx
157 and retina tissues, while controlling for confounding factors[29] (Methods). In cases where enrichment
158 was found, the number of eQTLs and sQTLs proposed to contribute to POAG risk and IOP variation
159 was estimated using an empirical true positive rate estimation approach (Fig. 1d and Methods). All
160 software and tools developed for this analysis were released on GitHub (see URLs).
161
162 **Colocalization analysis of POAG and IOP GWAS loci with e/sQTLs.** To identify a
163 comprehensive set of putative causal genes for POAG and IOP, we applied the colocalization
164 methods, eCAVIAR[34] and *enloc*[35], to 127 POAG loci from a large cross-ancestry GWAS meta-
165 analysis[8] (POAG CA), 68 POAG loci from a European subset meta-analysis[8] (POAG EUR), and
166 133 IOP loci from a primarily European GWAS meta-analysis[9] (IOP) (variant list in Supplementary
167 Table 1; Methods). All *cis*-eQTLs and *cis*-sQTLs in any of the 49 GTEx tissues (v8)[29] and *cis*-eQTLs
168 in peripheral retina[32,33], whose e/sVariants overlapped with each GWAS locus LD interval were
169 tested (Methods). The results are presented per trait and colocalization method in Supplementary

170 Tables 2-7 and summarized in Supplementary Table 8, filtering out potential false positives (flagged
171 in last column in Supplementary Tables 2-7; see Methods and examples in Supplementary Fig. 1).
172 We defined a "comprehensive set" of putative causal genes and regulatory mechanisms for POAG
173 and IOP as those e/sGenes that were significant with at least one of the colocalization methods
174 (Colocalization posterior probability (CLPP) > 0.01 for eCAVIAR, and regional colocalization
175 probability (RCP) > 0.1 for *enloc* per the methods' recommendations[34,35] (Methods); Supplementary
176 Table 8). A "high confidence set" of proposed causal genes was defined based on significant
177 colocalization with both methods (Table 1 and Supplementary Table 9). Of note, we found that the
178 number of significantly colocalizing e/sGenes per tissue significantly correlated with tissue sample
179 size (coefficient of determination R^2=0.72, P=1x10^{-14}, Supplementary Fig. 2) that is also associated
180 with number of detected e/sQTLs per tissue[29], suggesting that e/sQTL discovery power is a driving
181 factor in tissue identity of the colocalizing e/sQTLs. We therefore primarily considered the causal
182 genes proposed by the colocalization analysis in downstream analyses and not the associated
183 tissues.

184 We found that 58% of all GWAS loci tested significantly colocalized with at least one eQTL
185 and/or sQTL based on eCAVIAR and/or *enloc*: 60% (76) of 127 cross-ancestry POAG GWAS loci,
186 53% (36) of the 68 European POAG loci and 59% (79) of the 133 IOP loci (Fig. 2a and
187 Supplementary Table 10). Two-fold more GWAS loci colocalized with ≥1 eQTL than with ≥1 sQTL
188 (54.6% vs. 28.4%), likely due to the larger discovery rate of eQTLs compared to sQTLs in GTEx[29].
189 For 21% of the POAG and IOP GWAS loci (69 loci total), significant colocalization was found for
190 the same e/sGene with eCAVIAR and *enloc* ('high confidence set' listed in Table 1 and
191 Supplementary Table 9). These high confidence genes included *TMCO1* (eQTL and sQTL),
192 *CDKN2B-AS1* (sQTL), *GAS7* (eQTL), and *LMX1B* (eQTL), which colocalized with the largest
193 association signals for both POAG and IOP GWAS loci (Table 1, Supplementary Fig. 3-6, and
194 Supplementary Table 9). Hereafter, all downstream analyses are based on the comprehensive set
195 of mapped genes.

196 The GWAS-e/sQTL colocalization analysis significantly reduced the number of putative
197 causal genes per GWAS locus for POAG and IOP from an average of 22.8 ± 1.8 genes tested per
198 LD interval (range: 3-166, median=15) to an average of 3.5 ± 0.4 genes per locus (range: 1-36,
199 median of 1 or 2 genes per locus per trait; Fig. 2b,c and Supplementary Table 11). eQTLs and
200 sQTLs nominated an average of 3 and 2 causal genes per locus, respectively, with partial overlap
201 of target genes between the colocalizing eQTLs and sQTLs (Fig. 2c and Supplementary Table 8).
202 A single causal gene was proposed for 80 (42%) of the POAG and IOP loci with significantly
203 colocalizing e/sQTLs (Supplementary Tables 12 and 13), 49 (61%) of which are the nearest gene

204 to the lead GWAS variant. In 30.3% (23/76), 16.7% (6/36) and 31.7% (25/79) of the POAG CA,
205 POAG EUR and IOP GWAS loci, respectively, with significant colocalization results, the
206 colocalizing e/sGenes were not the nearest gene to the lead GWAS variant, as observed for other
207 complex traits[29,30,38]. This emphasizes the importance of using e/sQTLs to prioritize putative causal
208 genes implicated by GWAS loci. In total, 228, 118, and 279 genes, including previously suggested
209 and novel ones, are candidate causal genes for POAG CA risk, POAG EUR risk, and IOP variation,
210 respectively (Supplementary Table 14), with a total of 459 genes proposed from the combined
211 datasets.
212
213 **Noncoding genes proposed as contributors to POAG risk.** While the majority of colocalizing
214 e/sGenes are protein coding (60-72% per trait), noncoding RNA genes make up 18-20% of the
215 proposed causal genes for POAG and IOP loci (Fig. 2d and Supplementary Table 15), half of which
216 are lincRNAs and half antisense genes. Noncoding genes were proposed as a sole potential causal
217 gene for 10 POAG or IOP loci, including the lincRNA *LINC01948* in POAG cross-ancestry locus
218 rs112142644 on chromosome 5, and *RP11-217B7.2*, a lnc-ABCA1-1:1 lincRNA, in the shared
219 POAG and IOP locus on chromosome 10 (rs2472494 and rs2472493, respectively)
220 (Supplementary Table 8). We further found that e/sQTLs acting on 14 pairs of protein coding genes
221 and their corresponding antisense gene colocalized in the same GWAS locus, including *HLA-F* and
222 *HLA-F-AS1* with POAG risk, *LPP* and *LPP-AS2* with IOP levels, and *MAPT* and *MAPT-AS1* with
223 both POAG and IOP (Supplementary Table 16).
224
225 **Colocalizing e/sGenes of top POAG and IOP GWAS loci and direction of regulatory effect**
226 **on disease risk.** In addition to prioritizing causal genes and regulatory mechanisms that may
227 contribute to POAG and IOP, e/sQTL-GWAS fine-mapping and colocalization analysis proposes
228 the direction of effect of gene expression or splicing on disease risk or trait variation (examples for
229 top POAG and IOP GWAS signals in Fig. 3 and Supplementary Fig. 3). For example, of 13 or 27
230 e/sGenes tested for the second strongest association with POAG (rs2790053, odds ratio
231 (OR)=1.35) and the top IOP association (rs116089225, beta=-0.744), respectively, an eQTL and
232 sQTL acting on *TMCO1*, a gene that encodes a calcium channel localized to the endoplasmic
233 reticulum, and an eQTL acting on *TMCO1*'s antisense, *RP11-466F5.8*, in the opposite direction,
234 colocalized with POAG (CLPP=0.92-1) and IOP (CLPP=0.87-1) association signals (Fig. 4a-e and
235 Supplementary Fig. 4). Decreased expression of *TMCO1* and increased expression of *RP11-*
236 *466F5.8* are proposed to lead to increased IOP levels and increased risk of POAG (Fig. 4,
237 Supplementary Fig. 4, and Supplementary Table 8). Furthermore, an alternative splice donor site

238 in exon 4, the first exon in the *TMCO1* mRNA in GTEx Cells Cultured fibroblasts, which leads to a
239 longer exon 4 (Fig. 4f,g), is associated with decreased POAG risk (Supplementary Tables 2 and
240 8). Other examples include *ANGPT1* and *ANGPT2*, involved in vascular biology, whose increased
241 expression is proposed to reduce IOP levels (Supplementary Fig. 7 and Supplementary Table 8).
242 Interestingly, the eQTL acting on *ANGPT1* in Brain cerebellar hemisphere colocalized (RCP=0.23)
243 with the secondary IOP signal rs4496939 (chr8:107422472:A:G, beta = -0.118, $P=2.7x10^{-18}$;
244 Supplementary Fig. 7c,d) and not the strongest signal rs2022945 (chr8:107238911:G:A, beta = -
245 0.213, $P=1.1x10^{-28}$; Supplementary Fig. 7e), of the three independent signals in the locus.
246
247 **Colocalizing genes for shared and distinct POAG and IOP loci.** We found that of 50 overlapping
248 POAG and IOP GWAS loci, 39 (78%) of the loci had at least one significant colocalization result for
249 both traits, and in all cases at least one common gene was implicated (Supplementary Table 8 and
250 Table 1). In most of the cases (95%), the relative direction of effect of the colocalizing e/sQTLs on
251 IOP was consistent with IOP's effect on POAG risk, proposing IOP-dependent mechanisms for
252 POAG risk (Table 1 and Supplementary Table 8). For example, decreased *GAS7* expression or
253 increased *ABO* expression were associated with both increased IOP levels and increased POAG
254 risk (Supplementary Tables 2-8 and Supplementary Figs. 6,8). In the few cases where the direction
255 of effect was not consistent with IOP effect on POAG the colocalizing e/sQTLs were in different
256 tissues for the IOP and POAG GWAS loci.
257 To date, only a few loci have been found to be associated with NTG[8,39]. The strongest NTG
258 association (9p21) in the POAG CA (rs944801 OR=1.26) and POAG EUR (rs6475604 OR=1.3)
259 GWAS meta-analyses, not associated with IOP, significantly colocalized with a *CDKN2A* eQTL in
260 Brain Cortex, and *CDKN2B-AS1 and RP11-149I2.4* sQTLs in pituitary. In addition, a *CDKN2B*
261 eQTL in skeletal muscle colocalized with POAG in the EUR GWAS subset. These results imply
262 that increased expression of *CDKN2A* and decreased expression of *CDKN2B* may increase POAG
263 risk, exons 2 and 3 skipping in *CDKN2B-AS1* may increase POAG risk (Supplementary Fig. 3a and
264 Fig. 5), suggesting an IOP-independent molecular mechanism for POAG related to cell cycle
265 regulation.
266
267 **Colocalizing genes in population-specific and cross-ancestry POAG loci.** Most of the POAG
268 EUR loci (59 out of 68 loci) were found in the POAG cross-ancestry meta-analysis (Supplementary
269 Table 8). For 31 of these loci where a significant colocalization result was found for both the EUR
270 and CA GWAS, at least one common colocalizing e/sGenes was found between both GWAS. One
271 such example is *EFEMP1*, in which rare mutations have been associated with a mendelian form of

272 glaucoma[40]. Colocalization analysis suggests that skipping of exons 6 and 7 in *EFEMP1* that
273 encode epidermal growth factor (EGF)-like domains may be protective for POAG (Supplementary
274 Fig. 9). Of the nine loci found only in the POAG EUR GWAS, two loci colocalized with eQTLs acting
275 on several genes including genes involved in the extracellular matrix (*EMID1*) and vascular
276 endothelial growth (*ANGPTL2*), respectively, both of which also colocalized with IOP
277 (Supplementary Table 17). In addition, three associations in the POAG CA meta-analysis
278 demonstrated significant allelic heterogeneity among the three populations (European, East Asian,
279 and African American). e/sQTL colocalized with two of these loci. One is the 9p21 locus rs944801
280 with *CDKN2A/B* described above, that was significant in the European and Asian populations, but
281 not the African population in which it is in lower frequency (MAF=0.073 in gnomAD (URLs);
282 P_heterogeneity=1.5 x 10^{-8})[8].
283 The other European-specific locus in POAG CA GWAS with a significant colocalization
284 result was the POAG association with the largest odds ratio (OR=5.47) rs74315329, which is a
285 nonsense mutation (p.Gln368Ter) in *MYOC*, a gene encoding myocilin and associated with
286 hereditary juvenile-onset open-angle glaucoma. This variant is 10-fold more common in the
287 European population compared to the African population and is not found in the East Asian
288 population (gnomAD; URLs). Testing all e/sQTL gene-tissue pairs that overlapped this locus
289 targeting 24 genes identified an sQTL (chr1:172398537:A:G) acting on *PIGC,* phosphatidylinositol
290 glycan anchor biosynthesis class C, in spleen with eCAVIAR (CLPP=0.12) or artery tissue with
291 *enloc* (artery tibial, RCP=0.34; heart atrial appendage RPC=0.26) that significantly colocalized with
292 the POAG CA locus (splicing event: chr1:172370311-172376554; Supplementary Table 8 and
293 Supplementary Fig. 10). Since the nonsense variant in *MYOC* is likely the primary causal variant
294 in the locus, we tested whether a secondary haplotype may exist in the locus and, if so, if it
295 colocalizes with the *PIGC* sQTL. We performed association testing of all variants in the GWAS
296 locus LD interval conditioning on the lead POAG variant rs74315329 using COJO (Methods), and
297 found two low frequency, intronic variants that passed genome-wide significance
298 (chr1:171531082:A:G EUR MAF=0.0036 and chr1:170716994:A:C EUR MAF=0.002) and another
299 LD-independent signal (chr1:172398537:A:G, POAG GWAS conditional P=1.08x10^{-6}, EUR
300 MAF=0.075 in gnomAD) that passed Bonferroni correction for the number of variants tested in the
301 locus (P<5.87x10^{-6}) (Supplementary Table 18). We next tested whether the residuals of this
302 secondary signal, which are independent of the locus' lead variant rs74315329, colocalized with
303 any of the e/sQTL-tissue pairs in the locus using eCAVIAR and *enloc*. We found suggestive
304 significance (CLPP=0.009) for the POAG LD-independent signal chr1:172398537:A:G and the
305 same *PIGC* sQTL in spleen as above (chr1:172370311-172376554), as well as for a *PRRX1* eQTL

306 (CLPP=0.01) with eCAVIAR (Supplementary Tables 19-20), and significant colocalization for the
307 same *PIGC* sQTL in several tissues with *enloc* (maximum RCP=0.13) (Supplementary Tables 21-
308 22). *Enloc* also found significant POAG colocalization for another sQTL acting on *PIGC* (max
309 RCP=0.22, chr1:172376636-17237813) and for *PIGC* eQTLs (RCP=0.14) in several tissues
310 (Supplementary Tables 21-22). These results suggest that decreased exon 2 skipping in *PIGC*
311 (Supplementary Fig. 10) or increased *PIGC* expression may lead to increased POAG risk. In the
312 single cell analysis below, we found that *PIGC* is among 10 colocalizing POAG genes enriched in
313 oligodendrocytes in the optic nerve head (FDR=0.03; Supplementary Fig. 14c,d).
314
315 **Enrichment of POAG and IOP colocalizing e/sGenes in biological processes.** To gain
316 biological insight into ways the implicated genes might contribute to pathogenesis, we next asked
317 whether the target genes of all the colocalizing e/sQTLs with POAG CA, POAG EUR, or IOP GWAS
318 loci were enriched in specific biological pathways, gene ontologies, or mouse phenotype ontologies
319 using *GeneEnrich* (Methods). Genes that colocalized with POAG CA loci were significantly
320 enriched in elastic fiber formation (Empirical P-value (P)<$1x10^{-5}$, false discovery rate (FDR)<0.001)
321 and extracellular matrix organization (P=$3x10^{-5}$, FDR=0.012) correcting for multiple hypothesis
322 testing, and displayed nominal enrichment (P<0.05) in the transforming growth factor beta (TGF)
323 receptor signaling pathway (P=$3x10^{-4}$) and abnormal eye morphology (P=$2.6x10^{-3}$), amongst others
324 (Supplementary Table 23 and Supplementary Fig. 11a,b). No significant enrichment was found at
325 FDR<0.1 for e/sGenes colocalizing with POAG EUR loci. Top ranked nominal enrichment (P <
326 $4x10^{-3}$) for POAG EUR loci was found in cellular senescence and cell cycle processes (e.g., Cyclin
327 D-associated events in G1), lipid related processes, such as apolipoprotein binding and decreased
328 circulating high-density lipoprotein cholesterol level, and retina or neuronal related processes,
329 including abnormal retina morphology, abnormal sensory neuron innervation pattern, and negative
330 regulation of axon extension involved in axon guidance, amongst others (Supplementary Table 24
331 and Supplementary Fig. 11c,d).
332 For the IOP genes significant enrichment (P=$2x10^{-5}$, FDR=0.025) was found in
333 transcriptional regulation by *VENTX*, a gene that encodes a homeodomain-containing transcription
334 factor (Supplementary Table 25 and Supplementary fig. 11e). *VENTX* and its IOP-colocalizing
335 target genes driving the gene set enrichment signal (*ANAPC1*, *ANAPC7*, *AGO4*, *MOV10*, *TCF7L2*)
336 were most highly expressed in immune cell types, lymphocytes and macrophages, in the single cell
337 anterior segment and optic nerve head described below (Supplementary Fig. 11f). The IOP genes
338 were also significantly enriched (FDR<0.15) in blood vessel morphogenesis and vasculature
339 development, regulation of cytoskeletal organization, negative regulation of cellular component

340 organization, and adherens junction (Supplementary Table 25 and Supplementary Fig. 11e). Since
341 colocalization with multiple e/sQTLs was found for two loci in the HLA region on chromosome 6
342 (2.78 Mb apart) associated with POAG and IOP (29 and 35 e/sGenes, respectively), likely due to
343 high LD in the HLA region, we removed this region from the gene set enrichment analysis above
344 to avoid inflating the results due to a single locus. When kept in, the endosomal vacuolar pathway,
345 interferon gamma signaling, antigen presentation folding assembly and peptide loading of class I
346 MHC, negative regulation of natural killer cell mediated immunity, and cell aging were significantly
347 enriched (FDR<0.1) for POAG genes (Supplementary Table 26), in addition to the gene sets above.
348 The colocalizing POAG and IOP genes driving the gene set enrichment signals are listed in
349 Supplementary Tables 23-26.
350
351 **Identifying pathogenic cell types for POAG and related ocular traits.** To further relate the
352 implicated genes to pathogenic mechanisms and cell types, we next tested whether the expression
353 of the e/sGenes that colocalized with POAG or IOP or that mapped to GWAS loci of several other
354 related traits (listed in Supplementary Table 27) was enriched in specific cell types in key eye
355 tissues implicated in the pathophysiology of POAG: the anterior segment of the eye, where
356 impaired aqueous humor outflow can lead to elevated IOP, the retina, where death or dysfunction
357 of RGCs lead to POAG, and the optic nerve head, where local compression can cause axonopathy.
358 We first applied ECLIPSER[36,37] (see Methods) to 228, 118, and 279 e/sGenes that colocalized with
359 POAG CA, POAG EUR and IOP GWAS loci, respectively (Supplementary Table 8), and to cell
360 type-specific expression from single nucleus (sn) RNA-seq of (i) 6 tissues from the anterior
361 segment: central cornea, corneoscleral wedge (CSW), trabecular meshwork (TM) and Schlemm's
362 canal, iris, ciliary body (CB), and lens[28], (ii) the peripheral and macular retina, and (iii) the optic
363 nerve head (ONH) and adjacent retina[41], all taken from non-diseased human eyes (see Methods
364 and Supplementary Tables 28-30). The cell type enrichment results are summarized in
365 Supplementary Table 31.
366 In the anterior segment, we found significant enrichment (tissue-wide FDR<0.1) for POAG
367 EUR loci in fibroblasts derived from the ciliary muscle (present in CB, CSW and TM[28]), that were
368 annotated as ciliary fibroblasts in van Zyl *et al.*[28], and fibroblasts derived from the iris root (present
369 within the iris[28]), annotated as iris fibroblasts[28] (Supplementary Table 31 and Fig. 5a,b). The ciliary
370 muscle and iris are key tissues involved in the unconventional outflow pathway. These fibroblasts
371 were also detected histologically within the TM where all three tissues meet and interweave at the
372 iridocorneal angle[28], implicating the conventional aqueous outflow pathway as well. Fig. 5c shows
373 the e/sGenes driving the POAG EUR enrichment signal in ciliary fibroblasts. The POAG EUR genes

374 were only modestly enriched in fibroblasts derived predominantly from the TM tissue (annotated as
375 TM fibroblasts[28]) (FDR=0.18). We found supportive nominal enrichment (P<0.05, FDR<0.25) for
376 e/sGenes that colocalized with POAG CA loci in the ciliary (Supplementary Fig. 12) and iris
377 fibroblasts, as well as cornea and TM fibroblasts, vascular endothelium (cluster 2 derived from TM,
378 CSW and CB tissues[28]), and lens epithelium (Supplementary Table 31 and Fig. 5a,d). Genes
379 whose e/sQTLs colocalized with IOP GWAS loci were significantly enriched (FDR<0.1) in pericytes
380 (cluster 2 that localizes to the CSW[28]), TM fibroblasts, and ciliary fibroblasts, and modestly enriched
381 (FDR<0.2) in lens equator epithelium, vascular and lymphatic endothelium, and Schlemm's canal,
382 whose dysfunction can lead to elevated IOP[42] (Supplementary Table 31 and Fig. 5e).

383 Clustering of the top ranked anterior segment cell types (P<0.05) for POAG and IOP,
384 separately, based on the overlap of genes driving the cell type enrichment, suggests two cell
385 classes affecting POAG - fibroblasts populating the unconventional and conventional outflow
386 pathways and vascular endothelium, and three cell classes for IOP - fibroblasts in both outflow
387 pathways, pericytes, and lymphatic endothelial cells (Fig. 5f,g). Between 45-78% of the genes
388 driving the POAG enrichment signals in the outflow fibroblast cell types are common between the
389 different fibroblasts (Fig. 5f), suggesting both shared and distinct genes acting in the conventional
390 and unconventional outflow pathways. The IOP genes driving the enrichment signal in pericytes
391 (Fig. 5h,i) were largely distinct from those enriched in vascular and fibroblast cell types (overlap 7-
392 33%; Fig. 5g), and were enriched in vasculature development ($P=3x10^{-5}$, FDR=0.075;
393 Supplementary Table 33), while the IOP genes driving the enrichment in TM fibroblasts
394 (Supplementary Fig. 12c,d) were highly shared with the IOP genes enriched in ciliary and iris
395 fibroblasts (overlap 64-88%; Fig. 5g). Notably, the enrichment of IOP genes in pericytes was
396 specific to IOP; half of the IOP loci driving the enrichment signal in pericytes were not associated
397 with POAG risk (asterisks in Fig. 5h).

398 We next tested for enrichment of POAG and IOP colocalizing e/sGenes in retina snRNA-
399 seq data (Supplementary Table 28) (Methods). We found significant enrichment of POAG CA
400 genes in astrocyte and Müller glia cells in retina (FDR<0.059; Supplementary Table 31 and
401 Supplementary Fig. 13). POAG EUR and IOP genes did not display significant cell type enrichment
402 in the retina that passed multiple hypothesis correction; the IOP genes were nominally enriched in
403 astrocytes (P=0.027, FDR=0.43; Supplementary Fig. 13). Half of the POAG CA genes driving the
404 enrichment in astrocytes and Müller glia cells were common (Supplementary Fig. 13d,e),
405 suggesting shared and distinct processes. The POAG genes driving the enrichment in astrocytes
406 were enriched in MAPK6/MAPK4 signaling ($P=1x10^{-5}$, FDR=0.01) and regulation of cell projection
407 organization ($P=3x10^{-5}$, FDR=0.15) (Supplementary Table 33). The POAG CA enrichment in Müller

408 glia and astrocytes replicated (FDR<0.06) in a separate snRNA-seq study of the macula (Methods;
409 Supplementary Table 31 and Supplementary Fig. 13f).

410 Finally, we tested for cell type-specific enrichment in the optic nerve head (ONH) using
411 samples that also contained adjacent retinal tissue (Methods; Supplementary Table 30). In this
412 dataset, we found the strongest enrichment for POAG CA genes in astrocytes (FDR=0.005),
413 followed by Müller glia, smooth muscle, melanocytes, vascular endothelium, Schwann cells,
414 mlCones (a mixed population of M-cones and L-cones), and oligodendrocytes (FDR<0.05; Fig 6a,b,
415 Supplementary Table 31 and Supplementary Fig. 14). For POAG EUR genes, significant
416 enrichment was found in Müller glia, oligodendrocytes, and astrocytes (FDR<0.1; Fig. 6c and
417 Supplementary Table 31), and for IOP genes in smooth muscle, astrocytes, Schwann cells, and
418 vascular endothelium (FDR<0.04; Fig. 6d, Supplementary Table 31, and Supplementary Fig. 14).
419 These results confirm roles for astrocytes and Müller glia noted above, and reveal roles for cell
420 types within the ONH, e.g., oligodendrocytes, Schwann cells, and smooth muscle.

421 Over half of the genes driving the enrichment signal of POAG genes in astrocytes in ONH
422 (Fig. 6e,f) and retina tissues from separate donors were common (e.g., *DGKG, PLCE1, LPP*,
423 GAS7, *YAP1*, *COL11A1, and ABCA1*; Supplementary Table 31). *DGKG*, diacylglycerol kinase
424 gamma, whose retina eQTL colocalized (CLPP=0.96) with POAG CA association (Fig. 6g),
425 displayed the strongest cell type specificity in astrocytes (Fig. 6e,f). Furthermore, half the POAG
426 genes driving the enrichment in Müller glia in ONH and retina were shared (e.g., *PLCE1, CTTNBP2,*
427 *YAP1, TSC22D2, CLIC5,* and *TRIB2*), and mostly distinct from the astrocyte-specific genes
428 (Supplementary Table 31). This analysis proposes genes that may be affecting POAG risk via
429 changes in gene regulation in astrocytes and/or Müller glia cells. The IOP genes driving the
430 enrichment in smooth muscle that is unique to ONH are shown in Supplementary Fig. 14e,f; these
431 genes were enriched for anchoring junction and cell substrate junction cellular components
432 ($P<2.3x10^{-4}$, FDR=0.072; Supplementary Table 33). The cell type expression profiles of all POAG
433 CA, POAG EUR and IOP colocalizing e/sGenes is shown in Supplementary Fig. 15, and a summary
434 of the cell types and pathways in which each of the POAG and IOP colocalizing e/sGenes are
435 enriched is presented in Supplementary Tables 34-36.

436 To further augment the POAG and IOP enrichment analysis, we tested for cell type
437 enrichment of genes mapped to GWAS loci of additional glaucoma associated traits, including
438 vertical-cup-to-disc ratio (VCDR), cornea hysteresis, and central cornea thickness (Methods) in all
439 three ocular tissues (Supplementary Table 31). Since e/sQTL colocalization analysis of these traits
440 was beyond the scope of this paper, we mapped putative causal gene/s to the loci of these traits if
441 they had e/sQTLs in LD with the lead GWAS variant (Methods). In the anterior segment, genes

442 mapped to central corneal thickness and corneal hysteresis were most significantly enriched in
443 corneal fibroblasts (FDR<0.007; Supplementary Fig. 16a,b), highlighting the specificity of the
444 POAG and IOP gene enrichment in the outflow pathway fibroblasts. The VCDR GWAS loci from a
445 well-powered GWAS that used deep learning (ML) to score the characteristics of 65,680 fundus
446 images[12] showed significant enrichment in the TM fibroblasts from the conventional outflow
447 pathway (FDR=0.02; Supplementary Fig. 16c). TM fibroblasts were also the top nominally enriched
448 cell type for a smaller VCDR GWAS where 23,899 fundus images were manually scored by
449 ophthalmologists[13] (P=0.0076, FDR=0.3; Supplementary Fig. 16d). In the retina, corneal hysteresis
450 displayed significant enrichment in Müller glia cells (FDR=0.067; Supplementary Fig. 16e,f), and
451 the ML-based VCDR loci in mlCones (M-cone and L-cone photoreceptors) and GABAergic
452 amacrine cells (FDR=0.07; Supplementary Fig. 16g,h). In the ONH, both central corneal thickness
453 and corneal hysteresis displayed significant enrichment (FDR<0.1) in smooth muscle and astrocyte
454 (Supplementary Fig. 16i,j) and central corneal thickness also in Müller glia and Schwann cells
455 (Supplementary Fig. 16i). Genes mapped to VCDR loci, on the other hand, were primarily enriched
456 in mlCones (FDR=0.007; Supplementary Fig. 16k,l), distinct from the POAG and IOP enrichment.
457 Of note, the cell type enrichments of the cornea-related and VCDR traits in retina and ONH were
458 driven by a small number of e/sGenes (Supplementary Table 31). In summary, our cell type
459 enrichment analysis proposed known and new causal genes for POAG and related ocular traits
460 that may be affecting glaucoma susceptibility through specific cell types in the anterior and posterior
461 parts of the eye (Supplementary Table 31).
462
463 **Identifying new genetic associations of regulatory effects on POAG and IOP.** As the GWAS
464 loci discovered to date for POAG and IOP explain only a small portion of the traits' heritability, we
465 tested whether eQTLs and sQTLs can help identify new trait associations with modest effects
466 beyond genome-wide significance, not yet detected due to insufficient GWAS sample sizes. To this
467 end, we tested whether eQTLs and sQTLs from 49 GTEx tissues and retina eQTLs were enriched
468 for multiple POAG or IOP associations (GWAS P<0.05) using *QTLEnrich*[30], which adjusts for
469 confounding factors and tissue sample size (Methods). In cases where enrichment was found, we
470 estimated the number of e/sQTLs that may be true associations with POAG or IOP based on an
471 empirical estimation of the true positive rate (π_1), which we implemented in *QTLEnrich* (see
472 Methods).
473 We found significant enrichment of POAG and IOP associations among both eQTLs and
474 sQTLs in most of the 49 GTEx tissues and retina (Bonferroni-corrected $P<5x10^{-4}$) (Supplementary
475 Tables 37-39), with stronger enrichment found for IOP compared to POAG (Fig. 7a-c; One-sided

476 Wilcoxon rank sum test $P<1.6x10^{-8}$). Notably, the relative contribution of sQTLs to POAG risk and
477 IOP variation, as measured by adjusted fold-enrichment and estimated true positive rate, was larger
478 than the relative contribution of eQTLs to these traits (One-sided Wilcoxon rank sum test $P<1.5x10^{-}$
479 ^{11} and $P<0.03$, respectively; Fig. 7a,b and Supplementary Table 37-39). However, the absolute
480 number of eQTLs proposed to contribute to POAG risk and IOP variation (average 258 to 606; max
481 1205) was 2-fold larger than the number of sQTLs proposed to contribute to POAG and IOP
482 (average 124 to 320; max 788) (Fig. 7c and Supplementary Table 37). For POAG CA, the strongest
483 enrichment of hundreds of associations among eQTLs was found in brain, lymphocyte, cells
484 cultured fibroblast, esophagus, and artery, and among sQTLs in kidney cortex, heart atrial
485 appendage, brain, glands, and adipose (Fig. 7d,e,g, Supplementary Fig. 17 and Supplementary
486 Table 38-39). For IOP, the strongest enrichment among eQTLs was found in brain, adipose, skin,
487 fibroblast, and artery, and among sQTLs in brain, glands and heart atrial appendage (Fig. 7f,
488 Supplementary Fig. 17 and Supplementary Table 38-39). The retina eQTLs were also enriched for
489 POAG and IOP associations ($P<1x10^{-5}$), though not among the top-ranking tissues. While the GTEx
490 tissues are non-ocular tissues, many of the most strongly enriched tissues share cell types that
491 may be pathogenic to glaucoma. For example, glial cells in brain may share e/sQTLs also present
492 in astrocytes or Müller glia cells in the retina, vasculature cells in artery may be a proxy for the
493 lymphatic vessels in the aqueous outflow pathway, and cultured fibroblasts may share genetic
494 programs with the fibroblast cells in the ocular outflow pathway. In all, this analysis suggests that
495 over a thousand common variants that affect gene expression or alternative splicing are likely to
496 contribute to POAG risk and IOP variation.
497
498 **Pathway analysis of e/sQTL target genes of top ranked POAG and IOP associations.** To
499 identify the true positive POAG and IOP associations, beyond genome-wide significance, over
500 noise amongst the enriched e/sQTLs, and to propose potentially new causal genes and pathways,
501 we searched for target genes of e/sQTLs with POAG or IOP GWAS P-values below 0.05 that were
502 enriched in biological pathways, gene ontologies, or mouse phenotype ontologies. Our underlying
503 hypothesis was that genes that contribute to complex traits will cluster in a limited set of biological
504 processes. We applied *GeneEnrich* to a selected set of tissues per trait that displayed the highest
505 adjusted fold-enrichment, controlling for gene expression levels in the given tissue (Supplementary
506 Table 40-41). We found significant enrichment of target genes of brain hippocampus sQTLs with
507 top ranked POAG CA associations in mitochondrial respiratory complex I (FDR<0.05), including
508 NADH dehydrogenase complex assembly and mitochondrial respiratory chain complex assembly,
509 which included newly proposed genes for POAG (e.g., *NDUFB2, NDUFB4, NDUFAF1, NDUFAF2,*

510 *NDUFAF6,* and *ATP5SL*), and the citric acid TCA cycle (FDR=0.9) (Supplementary Table 40).
511 Target genes of gastroesophageal junction eQTLs with top ranked POAG associations were
512 enriched (FDR<0.1) in metabolic processes, including glycosaminoglycan biosynthesis keratan
513 sulfate and limonene and pinene degradation. Target genes of brain spinal cord eQTLs enriched
514 for IOP associations were enriched in cellular amino acid catabolic metabolism, in particular,
515 histidine metabolism (FDR=0.03), and skin eQTLs with top ranked IOP associations were enriched
516 in dynactin binding that is involved in moving membrane vesicles along microtubules (FDR=0.07)
517 (Supplementary Table 41). This analysis identified novel genes that may influence POAG risk or
518 IOP via regulatory effects (listed in Supplementary Table 40-41), functioning primarily in metabolic
519 processes. Examining other types of functional relationships, such as co-regulation or protein-
520 protein interactions, might help identify additional glaucoma associations and genes.
521
522 **Discussion**
523
524 Here we present a systematic investigation of the underlying causal mechanisms, genes
525 and cell types of over 130 loci associated with POAG[8,9], the most common form of glaucoma, and
526 over 100 loci associated with its major risk factor, elevated IOP[9]. Our analysis integrated a variety
527 of datasets, including expression and splicing QTLs from 49 GTEx tissues[29] and retina[29,32], single-
528 nucleus expression data from three glaucoma-relevant ocular tissues - anterior segment[28], retina,
529 and optic nerve head, and the largest to date GWAS meta-analyses for these traits[8]. Using two
530 QTL/GWAS colocalization methods[34,35], we prioritized putative causal genes for ~60% of the POAG
531 and IOP GWAS loci. A similar fraction of GWAS loci with significant colocalization results has been
532 found for other complex diseases and traits[29,38]. For a quarter (80) of the POAG and IOP loci, a
533 single gene was proposed, ten of which are noncoding genes (lincRNA and antisense), suggesting
534 that transcriptional and post-transcriptional gene regulation contribute to glaucoma susceptibility.
535 For about a third of the GWAS loci, none of the proposed causal gene/s were the nearest gene to
536 the lead GWAS variant, similar to that observed for other complex traits[30,38,43]. This emphasizes the
537 importance of using e/sQTLs or other functional assays that link regulatory regions to distal target
538 genes[30,44–46] to prioritize causal genes underlying common variant associations.
539 Integrating e/sQTLs with POAG and IOP GWAS loci proposed both previously suggested[8]
540 and new biological processes for these traits. The POAG colocalizing genes, which included
541 several known mendelian, early onset glaucoma genes (*EFEMP1*[40,47] and *LTBP2*[48]), were most
542 strongly enriched in extracellular matrix organization and elastic fiber formation, as previously
543 reported[8]. Structural changes of the extracellular matrix in both the trabecular meshwork in the

544 outflow pathway and the optic nerve head have been associated with POAG[49]. Regulation by the
545 homeodomain transcription factor, VENTX, was the most significantly enriched gene set for IOP
546 genes, which has not yet been associated with glaucoma. VENTX is proposed to play important
547 roles during embryonic patterning (by homology), including in neural crest development[50], as well
548 as hematopoiesis, leukemogenesis, cellular senescence and macrophage differentiation[51]. Its
549 strongest expression in our single cell data was in lymphocytes in the anterior segment, and
550 macrophages in the optic nerve head, proposing a novel link between immune-related processes
551 and IOP levels. Reduced circulating endothelial progenitor cells has been reported in POAG
552 patients[52], which could explain impaired flow mediated vasodilation in POAG[53]. Additional
553 processes suggested to affect IOP regulation based on gene set enrichment analysis included
554 vascular development, as previously suggested[9], regulation of cytoskeleton organization, and
555 adherens junction, a cell-cell junction whose cytoplasmic face is linked to the actin cytoskeleton,
556 and that allows cells to respond to biomechanical forces, biochemical signals and structural
557 changes in the tissue microenvironment[54]. Inhibition of adherens junction regulation in trabecular
558 meshwork has been shown to modestly influence IOP levels in rabbits[55]. We also found modest
559 enrichment of POAG genes in neuronal-related processes, including genes affecting retinal
560 morphology, sensory neuron innervation pattern, and regulation of axon guidance. These genes
561 may represent IOP-independent mechanisms, which will need to be corroborated in future GWAS
562 with larger numbers of normal tension glaucoma cases.

563 In addition to prioritizing causal genes for POAG and IOP, e/sQTLs suggest the direction of
564 effect of gene expression changes or alternative splicing on disease risk that could inform drug
565 design. In this study, we provide various hypotheses of putative causal genes and regulatory
566 mechanisms that may affect POAG susceptibility in an IOP-dependent or independent manner, for
567 experimental follow up. For example, an increase in expression or alternative splicing of *TMCO1*,
568 a gene that regulates the balance of calcium ions inside the endoplasmic reticulum, or a decrease
569 in expression of *LMX1B*, LIM homeobox transcription factor 1 beta, that is essential for several
570 developmental processes including the anterior segment of the eye[56], were proposed to reduce
571 POAG risk and IOP levels, while alternative splicing of *CDKN2B-AS1* may affect POAG
572 independent of IOP. An sQTL acting on *CDKN2B-AS1*, which leads to skipping of exons 2 and 3
573 that overlap the *CDKN2B* gene on the opposite strand, is proposed as a potential mechanism of
574 action for the protective signal found in this gene[57]. Skipping of these exons might render the
575 *CDKN2B* antisense less efficient in forming a complex with the *CDKN2B* RNA. Our work also
576 suggested a potential secondary causal gene, *PIGC* for the strongest POAG association, a
577 nonsense mutation in *MYOC*, a result that will need to be replicated in a larger independent POAG

578 GWAS. The *MYOC* mutation causes aggregation of misfolded myocilin proteins in the trabecular
579 meshwork, which imay lead to elevated IOP levels[58]. The enrichment of *PIGC* (that encodes an
580 endoplasmic reticulum associated protein) along with other POAG colocalizing genes in
581 oligodendrocytes in the optic nerve head suggests a secondary causal role for this locus in RGC
582 function.

583 There are several reasons why we may not have found colocalizing e/sQTLs for 40% of the
584 POAG and IOP loci. First, some of the causal genes or regulatory effects may be specific to regions
585 in the eye or rare cell types for which we do not yet have representative e/sQTLs. Second, some
586 genes may affect POAG or IOP by perturbing processes only active during development or under
587 specific conditions or stimuli, not captured in adult tissues. Third, the causal variant may be another
588 type of molecular QTL not tested in this study, such as e/sQTL acting in *trans* or protein QTLs.
589 Fourth, some of the genetic associations may be tagging deleterious protein-coding variants[8].
590 Finally, there are several limitations to Bayesian colocalization methodologies[59,60]. Under-
591 estimation of enrichment of e/sQTLs in a given tissue in GWAS hits, used as a prior in the
592 colocalization analysis, or GWAS loci with modest effect sizes may lead to loss of power[59].
593 Furthermore, the choice of genotype reference panel used to compute LD for fine-mapping of the
594 GWAS and QTL loci may have an effect on colocalization sensitivity. We used GTEx as our
595 reference panel, whose European to African sample ratio is comparable to that of the POAG cross-
596 ancestry GWAS, but has substantially fewer East Asian samples[29]. We do not expect this to have
597 a significant impact on our colocalization results as most of the POAG loci were found to be shared
598 across populations[8], and the fraction of loci with significant colocalization results was similar
599 between the POAG cross-ancestry and European subset GWAS meta-analyses.

600 There are caveats to consider in interpreting the colocalization results. Colocalization
601 analysis identifies co-occurring GWAS and e/sQTL loci likely driven by the same causal
602 variant/haplotype, suggesting that change in expression or splicing of the QTL target gene is causal
603 to the GWAS trait (vertical pleiotropy). However, we cannot rule out the possibility that the causal
604 effect on POAG or IOP may be through another mechanism other than change in gene expression
605 (horizontal pleiotropy). Approaches such as Mendelian randomization[61,62] can be used to further
606 support a causal effect of colocalizing e/sQTLs on POAG and IOP.

607 By applying a novel method (ECLIPSER) to the colocalizing e/sGenes and single nucleus
608 expression data from glaucoma-relevant eye tissues, we provide support for previously implicated
609 cell types affecting POAG development, and shed light on less well-established or novel pathogenic
610 cell types for POAG and IOP. One of the unique features of ECLIPSER, compared to other single
611 cell enrichment methods[63–67] is that it identifies cell types that are specific to a given disease or

612 trait, compared to a range of unrelated complex diseases and traits. Our results found that gene
613 expression variation in the TM cells and Schlemm's canal cells in the conventional outflow pathway,
614 as well as the ciliary and iris fibroblasts in the unconventional outflow pathway, may both be key
615 contributors to IOP regulation and POAG risk. Since the role of the unconventional outflow pathway
616 in IOP homeostasis remains relatively understudied compared to that of the conventional
617 pathway[68], these findings may encourage further avenues of investigation. Lack of enrichment in
618 ciliary epithelium, which is thought to be a primary producer of aqueous humor[69] suggests that
619 blockage of aqueous flow is more likely to affect IOP and POAG than aqueous overproduction. The
620 enrichment of genes that mapped to VCDR GWAS loci in TM fibroblasts suggests that the
621 conventional outflow pathway may have a stronger effect on optic nerve anatomy than the
622 unconventional pathway. Furthermore, the enrichment of IOP genes in pericytes, many of which
623 are not currently associated with POAG, extends our understanding of how genetic variation may
624 be affecting IOP in the anterior segment. Pericytes are mural cells that wrap around the endothelial
625 cells that line capillary blood vessels. A recent study has found reduced capillary diameter and
626 impaired blood flow at pericyte locations in mouse eyes with high IOP[70].

627 In the peripheral and macular retina and optic nerve head, we found significant enrichment
628 for POAG colocalizing genes in astrocyte and Müller glia cells, which replicated in an independent
629 snRNA-seq macula study. Astrocyte and Müller glia are two types of macroglia cells that wrap
630 around axons of neurons, including RGCs, and play an important role in retinal homeostasis,
631 including metabolic supply and structural support, maintaining the extracellular environment of the
632 neurons, and neurotransmitter transmission. Müller glia, the most common glial cell in the retina,
633 span the entire retinal layer, while astrocytes are present only in the innermost layer of the retina.
634 Several studies in animal models and patients with glaucoma[71–73] have found that astrocytes and
635 Müller glia cells become reactive at early stages of glaucomatous conditions when RGCs are intact,
636 suggesting a role for macroglia in the initiation and progression of glaucoma. The POAG genes
637 driving the astrocyte enrichment included genes enriched in extracellular matrix organization
638 (*COL8A2*, *COL11A1*), TGF-beta signaling (*SMAD6*) and sterol or lipid binding (*DGKG, MOV10,*
639 *RORA*) (Supplementary Table 34-35). Structural changes in the extracellular matrix induced by
640 TGF-beta2 in the optic nerve head, as with the aqueous outflow pathway, have been correlated
641 with POAG and have been suggested to cause impairment of optic nerve axonal transport and
642 neurotrophic supply that could influence RGC degeneration[49]. Of note, astrocytes have been found
643 to be one of the major cell types isolated from human ONH[74] and make up 20% of the cells in our
644 ONH dataset.

645 The strongest enrichment of IOP colocalizing genes was in smooth muscle cells in the ONH.
646 These genes were enriched for cell substrate junction and anchoring junction cellular components,
647 suggesting a role in cytoskeleton-associated cell-cell adhesion and cell-extracellular matrix
648 adhesion. These muscle cells may be part of the lamina cribrosa (LC), a mesh-like structure where
649 unmyelinated RGCs pass through the sclera to exit the eye, as LC cells isolated from human ONH
650 were found to stain for alpha-smooth muscle actin[74,75]. Cells in the LC produce extracellular matrix
651 proteins to support the LC structure[75], and biomechanical strain on the LC, such as from elevated
652 IOP, is thought to be one of the causes of RGC degeneration[76,77]. Further investigation will be
653 needed to determine whether the muscle cells found in our ONH single nucleus data reside in the
654 LC or in other structures such as blood vessels. Of note, astrocytes are the other common cell type
655 found in the LC dissected from human ONH[75]. The IOP genes were also enriched in vascular
656 endothelial cells in the optic nerve head, suggesting that vascular structural abnormalities or
657 functional dysregulation of blood flow to the optic nerve and retina may be an important contributor
658 to POAG[78]. It is also possible though that the enrichment in the ONH vascular endothelial cells is
659 capturing causal mechanisms acting in the vascular endothelial cells in the anterior segment that
660 were enriched for three quarters of the same IOP genes as in ONH (8 out of 12 genes). Notably,
661 we did not find significant enrichment of POAG or IOP genes in RGCs, whose cell death is the key
662 characteristic of glaucoma, but rather in neuronal support cells. Furthermore, while several studies
663 have suggested that microglia, specialized macrophage-like cells, may affect RGC survival[79], we
664 did not find support for a causal role of microglia in POAG susceptibility, based on our analyses. In
665 all, our findings in retina and ONH propose cell types and biological processes that may be viable
666 targets for neuroprotective therapies.

667 A potential limitation of our GWAS-cell type enrichment method, ECLIPSER is that it
668 primarily considers genes whose expression is specific to one or few cell types within a tissue, and
669 not genes expressed at similar levels across most or all cell types, which may also contribute to
670 disease risk or trait variation. Future considerations of multiple modest associations genome-wide
671 may increase discovery power of pathogenic cell types for glaucoma.

672 When considering genome-wide associations beyond the known GWAS loci, we found
673 significant enrichment of hundreds of new genetic regulatory effects on POAG risk and IOP
674 variation, suggesting a primary role for transcriptional regulation in POAG susceptibility, as
675 observed for other diseases[29–32]. This analysis suggested that sQTLs may have a stronger relative
676 effect on POAG and IOP than eQTLs, even though a larger number of eQTLs likely contribute to
677 POAG risk. A similar pattern was found for other complex traits[29]. The top ranked tissues with the
678 strongest eQTL enrichment of POAG and IOP associations: brain, fibroblasts, and artery, were in

679 line with our GWAS cell type specificity enrichment results. The enriched GTEx e/sQTLs likely
680 capture shared genetic regulation with the actual pathogenic tissues for glaucoma, partly explained
681 by GTEx tissues containing cell types that are relevant to POAG pathogenicity (e.g., fibroblasts in
682 outflow pathway or neuronal support cells in retina), and partly due to shared regulation across cell
683 types and tissues. It is also possible that dysregulation in some of the non-ocular tissues may
684 themselves affect POAG risk. Retina eQTLs, while significantly enriched for POAG associations,
685 did not display the strongest fold-enrichment. This may be because the cell types in retina affecting
686 POAG risk may not be highly abundant in the tissue and thus their eQTLs may not be well captured
687 by bulk tissue RNA-seq. One such example may be the Müller glia cells suggested by our single
688 cell analysis to be pathogenic for POAG.
689 In conclusion, our work has generated new insights into POAG mechanisms, which could
690 inform the development of novel therapies targeting IOP reduction and neuroprotection. By
691 integrating genetic regulation and single cell expression in glaucoma-relevant ocular tissues with
692 GWAS summary statistics we have identified known and new causal genes and biological
693 processes; proposed key ocular cell types that may be pathogenic for glaucoma; and provided
694 evidence for the existence of hundreds of novel genetic associations of regulatory effects for
695 glaucoma. In the future, detection of e/sQTL in relevant eye tissues and at the cellular level[80,81] is
696 expected to provide a more complete picture of the causal molecular and cellular mechanisms of
697 POAG risk and IOP variation. The approach and methods presented in this study can be applied
698 to any complex disease or trait with available GWAS summary statistics and single cell data from
699 relevant tissues or cell types.
700
701 **Methods**
702
703 **GWAS datasets.** We applied colocalization and fine-mapping analysis to 127 GWAS loci identified
704 in the cross-ancestry POAG GWAS meta-analysis of 34,179 cases and 349,321 controls from
705 European, African, and East Asian populations[8], 68 GWAS loci from the GWAS meta-analysis of
706 the European subset of 16,677 POAG cases and 199,580 controls[8], and 133 LD-independent
707 GWAS variants in 112 loci from the IOP GWAS meta-analysis of 139,555 primarily UK Biobank
708 samples[9]. The GWAS meta-analysis summary statistics, which included p-value, effect size and
709 standard error, were obtained from the corresponding studies. Chromosome positions were lifted
710 over from genome build 37 (hg19) to hg38. Association results on chromosome X were only
711 available for the POAG GWAS meta-analyses (cross-ancestry and European subset).
712

713 **GTEx and EyeGEx QTL datasets.** *cis*-eQTLs and *cis*-sQTLs from 49 tissues from GTEx release
714 v8[29] and *cis*-eQTLs from peripheral retina[32] were used in this study. Summary statistics of all
715 variant-gene e/sQTL pairs tested in each of the 50 tissues, the significant e/sGenes and e/sVariants
716 at FDR<0.05, and the gene expression levels and LeafCutter[82] values are available for download
717 from the GTEx portal (URLs). The summary statistics of all variant-gene pairs tested per gene and
718 tissue was used as input to the colocalization analysis, and the LocusZoom[83] and LocusCompare
719 plots (URLs). Plots of exon and exon junction read counts were taken from the visualizations on
720 the GTEx portal (URLs). Gencode versions 26 and 25 were used for the GTEx v8 and EyeGEx
721 studies, respectively.
722
723 **Colocalization analysis.** To identify a high confidence set of genes and regulatory mechanisms
724 that may be mediating the functional mechanisms underlying known genetic associations with
725 POAG and IOP, we applied two Bayesian-based colocalization methods: eCAVIAR[34] and *enloc*[35].
726 These methods assess the probability that co-occurring GWAS and e/sQTL signals are tagging the
727 same causal variant or haplotype and are applied to GWAS and QTL summary-level statistics
728 enabling the analysis of large, well-powered GWAS meta-analyses, for which genotype data are
729 not available. For the *enloc* analysis, DAP-G[35] was used to perform fine-mapping of GWAS and
730 e/sQTL loci to estimate the posterior probabilities of each variant in each locus being the causal
731 variant, while eCAVIAR has the fine-mapping feature built in. We applied the two colocalization
732 methods to 127 POAG GWAS loci from a recent cross-ancestry GWAS meta-analysis, 68 POAG
733 GWAS loci from the European subset meta-analysis, and 133 independent IOP variants (112 loci)
734 from a primarily European study (described above). Z-scores from the GWAS and GTEx e/sQTL
735 studies, computed as the effect size (beta) divided by the standard error of the effect size for each
736 variant, were used as input into eCAVIAR and the fine-mapping method, DAP-G. For the retina
737 eQTLs, we computed the z-score from the variant association p-values assuming a chi-square
738 distribution with 1 degree of freedom.
739 All GWAS loci were tested for colocalization with all eQTLs and sQTLs from 49 GTEx
740 tissues[29] and peripheral retina[32] that had at least 5 e/sVariants (FDR<0.05) within the GWAS locus
741 LD interval. An LD window around each lead GWAS variant was defined as the chromosome
742 positions on either side containing variants within $R^2 > 0.1$, determined using 1000 Genomes
743 Project Phase 3[84] as the reference panel, and extending an additional 50kb on either side. For the
744 IOP and POAG EUR loci, LD was computed using only the European samples in 1000 Genomes
745 Project, while for the cross-ancestry POAG loci, LD was computed using the European, African,
746 and East Asian samples in 1000 Genomes. If a GWAS variant was not found in 1000 Genomes,

747 an LD proxy variant (R^2 > 0.8) was searched for in GTEx, and if not found, the nearest variant was
748 used. The interval boundaries and number of variants tested are reported in Supplementary Tables
749 2-8. eCAVIAR and enloc analyses were applied to all common variants (MAF>1%) that fell within
750 the GWAS LD intervals and were present in both the GWAS and e/sQTL studies. The effect allele
751 of the variants in each GWAS was aligned relative to the alternative (ALT) allele, as done in GTEx
752 and EyeGEx.

753 **eCAVIAR analysis.** eCAVIAR[34] is a probabilistic model that estimates the posterior
754 probability that the same variant is causal in overlapping GWAS and e/sQTL signals, accounting
755 for the uncertainty of LD and allelic heterogeneity. It simultaneously performs statistical fine-
756 mapping on the GWAS and e/sQTL signals to optimize integration. For the eCAVIAR analysis, we
757 assumed at most two independent causal variants per locus[29]. Only variants present in both the
758 GWAS and QTL studies were analyzed. LD matrices with R^2 values between all pairwise variant
759 comparisons per locus were computed for each GWAS locus LD interval (defined above), using
760 the GTEx whole genome sequencing (WGS) data from release v8 as the reference panel, and were
761 used for fine-mapping of all variants in the GWAS and e/sQTL loci. The genotypes from all 838
762 GTEx donors in v8[29], consisting of European (84%), African (12.3%), and East Asian (1.4%)
763 ancestries, were used for the LD calculations for the cross-ancestry POAG loci, and the European
764 subset (715 donors) was used for the European POAG and IOP loci. Due to computational
765 limitations, for GWAS LD intervals with more than 1000 variants, variants with e/sQTL p-values
766 below 0.05 were filtered out. GWAS-e/sQTL-tissue combinations with a colocalization posterior
767 probability (CLPP) above 0.01 were considered significant in this study, based on previous
768 simulations that suggested a high true positive rate and low false positive rate at CLPP > 0.01[34].
769 Colocalization analysis of the retina eQTLs was only performed using eCAVIAR.

770 ***enloc* analysis.** *enloc* (Enrichment estimation aided colocalization analysis)[35] is a Bayesian
771 hierarchical model used to determine the probability of colocalization of molecular QTLs with
772 GWAS signals, that consists of three steps: estimation of enrichment levels of QTLs among the
773 GWAS hits, fine-mapping using an empirical Bayes method (DAP-G)[35], and colocalization analysis
774 that estimates a regional colocalization probability (RCP) that is the sum of SNP-level colocalization
775 probabilities (SCPs) of all variants per GWAS locus. *enloc* does not limit the potential number of
776 independent causal variants. To estimate the posterior probability of causality (posterior inclusion
777 probabilities (PIPs)) of variants in the GWAS loci we applied DAP-G (URLs) to all variants in the
778 LD intervals defined above for the POAG cross-ancestry, POAG European, and IOP loci. For
779 several loci, we restricted the maximum model size parameter (-msize) to 5, which represents the
780 number of independent association clusters, due to memory limitations. DAP-G outputs were post-

781 processed, selecting all fine-mapped variants and their associated cluster number and PIP for each
782 GWAS locus which were inputted into *enloc*. For the GTEx e/sQTLs, we used similar DAP-G fine-
783 mapping results published for all e/sQTLs in 49 GTEx tissues that were computed using the
784 European subset of GTEx samples[38]. LD matrices were computed per GWAS locus using all GTEx
785 WGS samples for the POAG cross-ancestry loci and the subset of European individuals in GTEx
786 for the POAG EUR and IOP loci, as the reference panel. We used an LD-threshold of 0.75 (-
787 ld_control) that determines the strength of genotype correlation between variants that belong to a
788 given fine-mapped signal cluster, as used in the GTEx European subset e/sQTL analysis[38]. Finally,
789 we applied *fastEnloc*[85] (URLs), a faster implementation of *enloc*, to the fine-mapped results of the
790 GWAS loci and overlapping GTEx e/sQTLs. Only e/sVariants included in a 25% or greater credible
791 set of causal variants and that overlapped with the GWAS variants were analzyed in the
792 colocalization analysis. The colocalization analysis outputted RCP values above $1x10^{-4}$ for each
793 tested GWAS locus, trait, tissue, and gene or gene-intron excision cluster combination. An RCP
794 above 0.1 was considered significant in this study, based on the method's recommendation[35,59]. In
795 Supplementary Tables 5-7 we listed the set of variants included in the 95% credible set for each
796 independent GWAS locus, e/sQTL, gene and tissue colocalization signal (cluster). In cases where
797 a significantly colocalizing sQTL that regulates an intron cluster mapped to more than one gene,
798 all target genes were reported as significant.

799 **Quality control and summary across the two colocalization methods.** In inspecting the
800 significant colocalization results and plotting the $-\log_{10}$(P-value) of the GWAS signal versus the -
801 $\log_{10}$(P-value) of the e/sQTL signal, we noticed multiple cases where the GWAS P-values and/or
802 the e/sQTL P-values of the variants with significant colocalization posterior probabilities
803 (CLPP>0.01 and/or RCP>0.1) were not significant (e.g., association P>0.05) or did not pass
804 multiple hypothesis correction (see examples in **Supplementary Fig. 1**). Thus, to remove potential
805 false positives, we filtered out variant, gene, tissue, trait combinations where the e/sVariant with a
806 significant colocalization result had a GWAS p-value above $1x10^{-5}$ or whose e/sQTL p-values was
807 above $1x10^{-4}$ and/or did not pass FDR<0.05 (FALSE in column
808 'Pass_QC_QTL_FDR05_P1E04_GWAS_P1E05' in **Supplementary Tables 2-7)**. We chose a
809 GWAS $P<10^{-5}$ cutoff, as it has been suggested that in many cases the lead GWAS variant is not
810 the causal variant, but instead tagging the causal variant that may have not reached genome-wide
811 significance[86]. We defined two sets of putative causal genes and regulatory mechanisms for POAG
812 and IOP: a "comprehensive set" based on significant colocalization with at least one of the
813 colocalization methods (CLPP > 0.01 and/or RCP > 0.1) (Supplementary Table 8), and a "high
814 confidence set" based on significance with both methods (CLPP > 0.01 and RCP > 0.1; Table 1

815 and Supplementary Table 9). Since the number of significantly colocalizing e/sGenes correlated
816 with the tissue sample size (coefficient of determination R^2=0.72, P=1x10^{-14}, Supplementary Fig.
817 2), we disregarded the tissue and only considered the QTL type and e/sGene when generating the
818 list of prioritized causal genes per GWAS locus.
819
820 **Single nucleus RNA-seq datasets and differential gene expression.** We analyzed gene
821 expression values (log(TPK+1)) from four single nucleus (sn) RNA-seq data sets from the following
822 glaucoma-relevant regions of the eye: anterior segment, retina, and optic nerve head. All tissue
823 samples were dissected from non-diseased eye globes from post-mortem donors with no record of
824 eye disease, and were de-identified. Here is a description of the four datasets:
825 **Anterior segment:** Six tissues in the anterior segment, including central cornea,
826 corneoscleral wedge (CSW), trabecular meshwork (TM), iris, ciliary body (CB) and lens, were
827 dissected from six donors within 6 hours from death, as described in[28]. To be able to compare
828 across cell types between tissues in the anterior segment, the snRNA-seq data from cornea, CSW,
829 CB, iris, and TM were pooled, downsampled to 1000 cells per type in each tissue, and reclustered
830 yielding 34 clusters[28]. Five clusters were identified for the lens. Differential gene expression
831 analysis between each cell type and all other cell types was performed using the regression model
832 in MAST[87] that corrects for the proportion of genes expressed per cell. Only genes expressed in
833 more than 25% of cells in any cluster and with $\log_2$(fold-change) above 0.25 were included in the
834 analysis.
835 **Retina**: Retina samples from the fovea, macula and/or periphery were collected from six
836 donors within 6 hours from death from the Utah Lions Eye Bank (Supplementary Table 28). The
837 number of cells from the three retinal regions from each donor is given in Supplementary Table 28.
838 The fovea (with central macula) and macula samples were collected separately, using a 4 mm and
839 6 mm disposable biopsy punch, respectively, and were flash-frozen in liquid nitrogen. snRNA-seq
840 data from RGCs from a few additional donors were added to the data set, given the relevance of
841 RGCs to glaucoma, though RGCs still only comprised about 1/250 of the total data set. Nuclei were
842 isolated by pre-chilled fresh-made lysis buffer (10 mM Tris-HCl, 10 mM NaCl, 3 mM MgCl2, 0.02%
843 NP40). The frozen tissue was triturated to break the tissue structure in lysis buffer and
844 homogenized with a Wheaton™ Dounce Tissue Grinder. For the nuclei to be enriched, isolated
845 nuclei were stained with mouse anti-NeuN monoclonal antibody in pre-chilled wash buffer (1% BSA
846 in PBS, 0.2U/µl RNAse inhibitor) for 30min at 4°C. After being centrifuged at 500g, the pellet was
847 resuspended in wash buffer and filtered with 40µm Flowmi Cell Strainer. DAPI (4′,6-diamidino-2-
848 phenylindole, 10 µg/ml) was added before loading the nuclei for fluorescent cytometry sorting.

849 Stained nuclei were sorted with a FACS Aria II flow sorter (Becton Dickinson, San Jose, CA) (70μm
850 nozzle). Sorting gates were based on the strengths of DAPI signal and FITC signal. Samples were
851 sorted at a rate of 50 events per second. Fluorescence detection used a 450-nm/40-nm-band pass
852 barrier filter for DAPI, and a 530-nm/30-nm-band pass filter for FITC. All single-nuclei RNA
853 sequencing of the retina samples was performed at the Single Cell Genomics Core at Baylor
854 College of Medicine. Single-nuclei cDNA library preparation and sequencing were performed
855 following the manufacturer's protocols (https://www.10xgenomics.com). Single-nuclei suspension
856 was loaded on a Chromium controller to obtain single-cell GEMS (Gel Beads-In-Emulsions) for the
857 reaction. The snRNA-seq library was prepared with Chromium Next GEM Single Cell 3' Kit v3.1
858 (10x Genomics). The library was then sequenced on Illumina NovaSeq 6000
859 (https://www.illumina.com). Reads from snRNA-seq were demultiplexed and then aligned to the
860 'Ref_cellranger.hg19.premrna' human reference (from 10x Genomics) using Cell Ranger (version
861 3.0.2, 10x Genomics). The gene expression matrices were generated by the Cell Ranger pipeline.
862 For each matrix, genes detected in less than 5 cells were removed; cells with total UMI counts less
863 than 500 were removed, and the top 5% of cells with the highest mitochondrial gene expression
864 proportion were removed. We then performed doublet removal on the remaining cells using
865 DoubletFinder. The gene expression was then normalized by total UMI counts for each cell, scaled
866 by 10000, and transformed with the natural logarithm. To account for batch effects originating from
867 sample collection processes, the CarDEC framework[88] was applied with standard parameters. Both
868 highly variable genes (top 3000) and lowly variable genes were used for building the model, and
869 donor resources were used as the batch key. The low dimensional embeddings generated were
870 then used to perform leiden clustering, and major cell types were annotated based on known
871 marker genes (GNAT1, PDE6A for rod; ARR3, PDE6C for cone; RLBP1, GLUL for MG; C1QA,
872 C1QB for microglia; GFAP for astrocyte; RPE65, LRAT for RPE). Differential gene expression for
873 each cell type in the ml_class level used in this study was computed using the Wilcoxon rank sum
874 test, applied to genes expressed in at least 10% of cells per cell type and with a $\log_2$(fold-change)
875 above 0.25.

876 **Macula:** Macular samples were dissected with 8mm punches from five donors within 4
877 hours of death at the University of Utah (Supplementary Table 29). For three of the samples, RGCs
878 were enriched by staining the nuclei with NENU antibody (Millipore Sigma, #FCMAB317PE)
879 followed by FACS sorting. The macular samples were processed similarly to the optic nerve head
880 samples below. Differential gene expression for each cell type compared to all other cell types was
881 computed using the MAST method[87], considering only genes expressed in more than 25% of cells
882 in any cell type and $\log_2$(fold-change) above 0.25.

883 **Optic nerve head:** The optic nerve head, including parapapillary tissues, was dissected
884 with 4 mm punches from six donors within 4 hours of death at the University of Utah and
885 Massachusetts General Hospital (Supplementary Table 30). Tissues were frozen and kept at -80C.
886 For single-nuclei isolation, frozen tissues were homogenized in a dounce homogenizer with 0.1%
887 NP-40 lysis buffer and passed through a 40-µm cell strainer. The nuclei were then pelleted at 500
888 rcf over 5 min, resuspended in 2% BSA, and stained with DAPI. ~40K DAPI+ nuclei were sorted
889 and pelleted at 500 rcf over 5 min. Finally, nuclei were resuspended in 0.04% non-acetylated
890 BSA/PBS solution and adjusted to a concentration of 1000 nuclei/µL. The integrity of the nuclear
891 membrane, protrusion of nuclear content, and presence of non-nuclear material were assessed
892 under a brightfield microscope. Nuclei were then loaded into a 10X Chromium Single Cell Chip with
893 a targeted recovery of 8000 nuclei. Single nuclei libraries were generated with Chromium 3' V3.1
894 platform (10X Genomics, Pleasanton, CA) following the manufacturer's protocol. Briefly, single
895 nuclei were partitioned into Gel-beads-in-EMulsion (GEMs) where nuclear lysis and barcoded
896 reverse transcription of RNA would take place to yield full-length cDNA; this was followed by
897 amplification, enzymatic fragmentation, and 5' adaptor and sample index attachment to yield the
898 final libraries. The single nucleus RNA sequencing of the optic nerve head samples was performed
899 on NovaSeq machines at a Harvard University facility. snRNA data processing and analyses were
900 performed similarly to the pipeline used for the anterior segment in van Zyl *et al.*[28]. Differential gene
901 expression for each cell type compared to all other cell types was computed using the MAST
902 method[87], considering only genes expressed in more than 25% of cells in any cell type and $\log_2$(fold-
903 change) above 0.25.
904
905 **Cell type-specific enrichment of genes that map to GWAS loci for a given complex trait.** To
906 identify ocular cell types that are enriched for cell type-specific expression of genes mapped to
907 GWAS loci of POAG, IOP and several related traits, we extended a method we recently developed
908 called ECLIPSER (Enrichment of Causal Loci and Identification of Pathogenic cells in Single Cell
909 Expression and Regulation data)[36,37], to e/sQTL colocalizing genes. ECLIPSER assesses whether
910 genes mapped to a set of GWAS loci for a given complex disease or trait are enriched for cell type-
911 specific expression compared to the cell type specificity of genes mapped to a background (null)
912 set of GWAS loci associated with hundreds of unrelated traits. The analysis consisted of the
913 following main steps: **(i) Mapping genes to GWAS loci.** For the POAG and IOP traits, e/sQTL
914 colocalization was used to prioritize genes in GWAS loci. For the cornea-related traits and VCDR,
915 genes were mapped to GWAS loci if they were target genes of a GTEx or retina e/sQTL that was
916 in LD (R^2>0.8) with the GWAS locus (since colocalization analysis for these traits was beyond the

917 scope of this paper). The genome-wide significant variants associated with the cornea traits were
918 taken from Open Targets Genetics[89], and for physician and machine learning-based VCDR
919 measures from the corresponding published GWAS meta-analyses[12,13]. **(ii) Null set of GWAS loci.**
920 We compiled a null set of GWAS loci, by selecting all genome-wide significant associations for a
921 range of traits in Open Targets Genetics[89], that were taken from the NHGRI-EBI GWAS catalog
922 and UK Biobank GWAS studies. We excluded from the null set variants associated with any ocular
923 trait. **(iii) LD clumping of loci.** We collapsed GWAS variants that were in LD with each other
924 (R^2>0.8) or that shared a mapped gene into a single locus for the GWAS locus set of each ocular
925 trait and for the null set, separately, to avoid inflating the cell type enrichment results due to LD[37].
926 **(iv) Cell type specificity locus score.** We scored each GWAS locus for the ocular traits and the
927 null set as the fraction of genes mapped to the locus that demonstrated cell type specificity (defined
928 here as fold-change > 1.3 and FDR < 0.1). **(v) Assessing cell type-specificity of GWAS locus**
929 **set.** We estimated a cell type specificity fold-enrichment and p-value per trait (GWAS locus set),
930 tissue and cell type combination, compared to the null GWAS locus set, using a Bayesian Fisher's
931 exact test and the 95th percentile of the null locus scores for the cell type specificity cutoff. The
932 Bayesian approach enables estimating 95% confidence intervals of the fold-enrichment, including
933 for traits that have few or no loci that fall above the enrichment cutoff[37]. **(vi) Cell type specific**
934 **disease-contributing genes.** Cell type-specific genes mapped to GWAS loci whose score was
935 equal to or above the 95th percentile enrichment cutoff in significantly enriched cell types ('leading
936 edge loci'), were proposed to contribute to the given complex trait in the given cell type ('leading
937 edge genes'). Cell types with a tissue-wide Benjamini-Hochberg FDR equal to or below 0.1,
938 correcting for the number of cell types tested per tissue, were considered significantly enriched for
939 genes associated with a given trait.
940
941 **Enrichment of POAG and IOP associations among e/sQTLs using *QTLEnrich.*** To test whether
942 POAG and IOP trait associations, beyond genome-wide significance, are enriched among eQTLs
943 and sQTLs and to assess the contribution of e/sQTLs to these traits, we applied *QTLEnrich*[30] to
944 the POAG and IOP GWAS meta-analyses summary statistics, and eQTLs and sQTLs from the 49
945 GTEx tissues[29,32] and eQTLs from peripheral retina (EyeGEx[32]). *QTLEnrich* is a rank and
946 permutation-based method that evaluates the fold-enrichment significance of trait associations
947 among a set of e/sQTLs in a given tissue, compared to a tissue-specific null distribution of variants
948 matched on three confounding factors: minor allele frequency (MAF), distance to the target gene's
949 transcription start site, and local LD[30]. Briefly, fold-enrichment was computed for each trait by
950 e/sQTL-tissue combination as the fraction of e/sVariants (FDR<0.05) with a GWAS P-value<0.05

compared to expectation, assuming a uniform null distribution. Fold-enrichment was also computed for $<10^5$ randomly sampled sets of *k* null variants (non-significant e/sVariants; *k* = number of significant e/sVariants in given tissue) matched on the three confounding factors relative to each significant e/sVariant. Random sampling was applied to decile bins of the confounding factors with replacement. The null background of variants was defined as all common variants (MAF>1%) tested for e/sQTL in GTEx or retina excluding the significant e/sVariants (FDR<0.05). The enrichment p-value was computed as the fraction of up to 10^5 null variant sets whose fold-enrichment was equal to or higher than that of the significant set of e/sVariants for a given tissue. To adjust for the potential enrichment of trait associations amongst null variants, an adjusted fold-enrichment was computed per trait-e/sQTL-tissue combination as the observed fold-enrichment divided by the median fold-enrichment of 1000 confounder-matched null variant sets. Local LD was estimated based on the number of LD proxy variants ($R^2 > 0.5$) per variant, using GTEx WGS v8 VCF as the reference panel. For the enrichment analysis only the most significant e/sVariant per e/sGene (FDR<0.05) in the given tissue was used to prevent inflation of trait association enrichment due to LD. In cases where the e/sQTL was the most significant e/sVariant for more than one e/sGene, the smallest distance to TSS was used. Only protein coding and lincRNA genes were considered in this analysis. Significant tissues were determined based on an Enrichment P-value that passed Bonferroni correction, correcting for 50 tissues and two QTL types tested ($P<5x10^{-4}$). The adjusted fold-enrichment was used to rank the significantly enriched tissues, as this statistic is not correlated with tissue sample size or number of significant e/sQTLs per tissue[30], as observed with the colocalization analysis (Supplementary Fig. 2).

For the significant trait-tissue pairs, the fraction and number of e/sVariants proposed to be associated with POAG or IOP were estimated using an empirically derived, true positive rate (Adj. π_1) approach implemented in the latest version of *QTLEnrich* (URLs), based on Storey's analytical π_1[90,91] and an empirical FDR method[90,91]. The adj. π_1 adjusts for enrichment of trait associations amongst non-significant e/sQTL variants matched on confounding factors. A lambda of 0.8 was used to estimate the adjusted true negative rate. The estimated number of trait associations amongst a set of e/sVariants in a given tissue was computed as the adj. π_1 times the number of e/sQTLs analyzed for that tissue. In few cases, the adj. π_1 can be zero for e/sQTLs that display significant enrichment of trait associations. This may be caused by deflation of the GWAS p-values of the e/sQTL set at the higher end of p-values that are used to estimate the true negative rate. *QTLEnrich* thus also estimates a lower bound number of trait associations among e/sQTLs with GWAS P<0.05 that is not affected by this issue (Supplementary Tables 38-39).

985 **Gene set enrichment analysis of POAG and IOP associated genes.** We used *GeneEnrich*[29,30]
986 to test whether genes proposed to affect POAG risk or IOP variation in this study cluster in specific
987 biological processes or mouse phenotype ontologies. *GeneEnrich* assesses enrichment of a set of
988 genes of interest in biological pathways or other types of biologically meaningful gene sets, using
989 a hypergeometric distribution and permutation analysis. To account for biases that could arise from
990 the set of genes expressed in a given tissue, an empirical gene set enrichment P-value was
991 computed as the fraction of 1,000 to 100,000 *k* randomly sampled genes (*k* = number of significant
992 genes, e.g., colocalizing e/sGenes) from all genes expressed in the given tissue (background set)
993 that have a hypergeometric probability equal to or higher than that of the significant list of genes.
994 *GeneEnrich* has the option to match on expression levels of the significant set of genes when
995 randomly sampling genes from the background set, to ensure that significant gene set enrichment
996 is not driven by expression levels in the particular tissue. Given the high LD in the HLA region on
997 chromosome 6 (chr6:28510120-33480577) we removed all genes in this region from the gene set
998 enrichment analysis, unless noted otherwise.

999 We applied *GeneEnrich* to three groups of POAG and IOP associated genes: (i) All 228,
1000 118, and 279 unique target genes of eQTLs and sQTLs that colocalized with POAG CA, POAG
1001 EUR, and IOP GWAS loci, respectively. Given that the colocalizing e/sQTLs were derived from the
1002 different GTEx tissues and retina, we used all genes expressed in any of the 49 GTEx tissues and
1003 retina as the background set of genes, and did not correct for expression levels given the
1004 differences in expression levels between tissues. (ii) Sets of POAG and IOP colocalizing genes
1005 that were enriched in specific cell types in the eye tissues based on ECLIPSER analysis (tissue-
1006 wide FDR ≤ 0.1). For the background sets of genes, we chose all genes expressed in the GTEx or
1007 retina tissue that was relevant for the enriched cell type (e.g., Brain for Optic nerve head; full list in
1008 Supplementary Table 32). Given that the expression levels in a tissue may not fully reflect the
1009 expression levels in the particular cell type, we did not correct for expression levels in the gene set
1010 enrichment analysis of the cell type-specific gene sets. (iii) Target genes of e/sQTLs (FDR<0.05)
1011 with POAG or IOP GWAS P-value below 0.05 in tissues that were enriched for trait associations
1012 based on *QTLEnrich*. Given that e/sQTLs in most tissues displayed significant enrichment, a select
1013 set of QTL/tissue-trait pairs was chosen for gene set enrichment analysis based on the tissue
1014 having a top ranked adjusted fold-enrichment and consisting of cell types that may be relevant to
1015 glaucoma pathophysiology, such as cells cultured fibroblasts, brain, and artery. The background
1016 sets of genes were defined as all genes expressed in the given tissue whose most significant
1017 e/sVariant had a GWAS P-value above 0.05. Expression levels were adjusted for in the permutation
1018 analysis.

1019 We applied *GeneEnrich* to over 11,000 gene sets from four databases downloaded from
1020 MSigDB (URLs): Gene Ontology (GO) with three domains: biological processes, molecular
1021 function, and cellular components; Reactome; Kyoto Encyclopedia of Genes and Genomes
1022 (KEGG); and mouse phenotype ontology gene sets from the Mouse Genome Informatics (MGI).
1023 Only gene sets with 10 to 1000 genes were tested. Only genes that were found in the given
1024 database were included in the gene set enrichment analysis. Statistical significance was
1025 determined using a Benjamini Hochberg false discovery rate (FDR) below 0.1 per database, given
1026 extensive gene set overlap between databases. Gene sets with empirical gene set enrichment
1027 below 0.05 were considered nominally significant.
1028
1029 **Conditional analysis of *MYOC* POAG locus**. Given our finding of significant colocalization of a
1030 *PIGC* sQTL with the POAG cross-ancestry association signal in the GWAS locus rs74315329
1031 (chr1:171636338:G:A, MAF=0.0026, odds ratio=5.47) whose lead variant is a nonsense mutation
1032 in the *MYOC* gene, we tested whether there was a secondary independent signal in this locus that
1033 might colocalize with the *PIGC* sQTL. We performed association testing on all variants on
1034 chromosome 1 conditioning on rs74315329, the lead POAG GWAS variant in the locus by applying
1035 the tool COJO (URLs) to the POAG trans-ancestry GWAS meta-analysis summary statistics on
1036 chromosome 1. To maintain the *MYOC* lead variant in the initial association testing we filtered out
1037 variants with MAF<0.0001. The effective sample size of the POAG cross-ancestry GWAS was
1038 computed based on the equation: 4/[(1/Ncases)+(1/Ncontrols)][92], which yielded N=124,531 for the
1039 POAG GWAS cross-ancestry meta-analysis[8]. The variant allele frequencies required as input to
1040 COJO, we computed the minor allele frequencies per variant using the European, African and East
1041 Asian samples in 1000 Genomes Project, as the POAG GWAS meta-analysis is comprised of three
1042 ancestral groups. eCAVIAR and *enloc* were applied to the residual statistics in the *MOYC* locus
1043 from the conditional analysis and all overlapping e/sQTLs from the GTEx tissues and retina. To
1044 remove potential false positives, we filtered out variant, gene, tissue, trait combinations if the
1045 e/sVariant with a significant colocalization result had a GWAS p-value above $2x10^{-5}$ or an e/sQTL
1046 p-value above $1x10^{-4}$ and/or an FDR above 0.05 (FALSE in column
1047 'Pass_QC_QTL_FDR05_P1E04_GWAS_P2E05' in Supplementary Tables 19 and 21). We used a
1048 slightly more lenient GWAS p-value cutoff for the conditional analysis ($P<2x10^{-5}$ compared to
1049 $P<1x10^{-5}$ used for the original GWAS summary statistics) given the reduced association power of
1050 conditional analysis.
1051
1052 **Acknowledgements**

We thank William Wen for helpful discussions on the interpretation of the colocalization results. We thank members of the Segrè lab for valuable comments and feedback. This work was funded by NIH/NEI R01 EY031424-01 (AVS, ARH, JR, PAM), NIH/NEI P30 EY014104 (JLW, AVS), NIH/NEI EY032559-01 (JLW, AVS), and the Chan Zuckerberg Initiative (CZI) Seed Network for the Human Cell Atlas awards CZF2019-002459 and CZF2019-002425. XJ is supported by the University of Edinburgh and University of Helsinki joint PhD studentship program in Human Genomics. VV is supported by an MRC University Unit Programme grant (MC_UU_00007/10) (QTL in Health and Disease). All GTEx protected data are available through the database of Genotypes and Phenotypes (dbGaP) (accession no. phs000424.v8).

URLs

GTEx: https://gtexportal.org/home/datasets

EyeGEx: https://gtexportal.org/home/datasets

PLINK: https://www.cog-genomics.org/plink/

eCAVIAR: https://github.com/fhormoz/caviar

fastEnloc: https://github.com/xqwen/fastenloc

DAP-G: https://github.com/xqwen/dap/tree/master/dap_src

COJO: https://yanglab.westlake.edu.cn/software/gcta/

ECLIPSER: https://github.com/segrelabgenomics/ECLIPSER

QTLEnrich: https://github.com/segrelabgenomics/QTLEnrich

GeneEnrich: https://www.asegrelab.org/software

genomAD: https://gnomad.broadinstitute.org/

MSigDB: http://www.gsea-msigdb.org/gsea/msigdb/collections.jsp

QMplot: https://github.com/ShujiaHuang/qmplot

LocusCompare: https://github.com/boxiangliu/locuscomparer

Figure 1

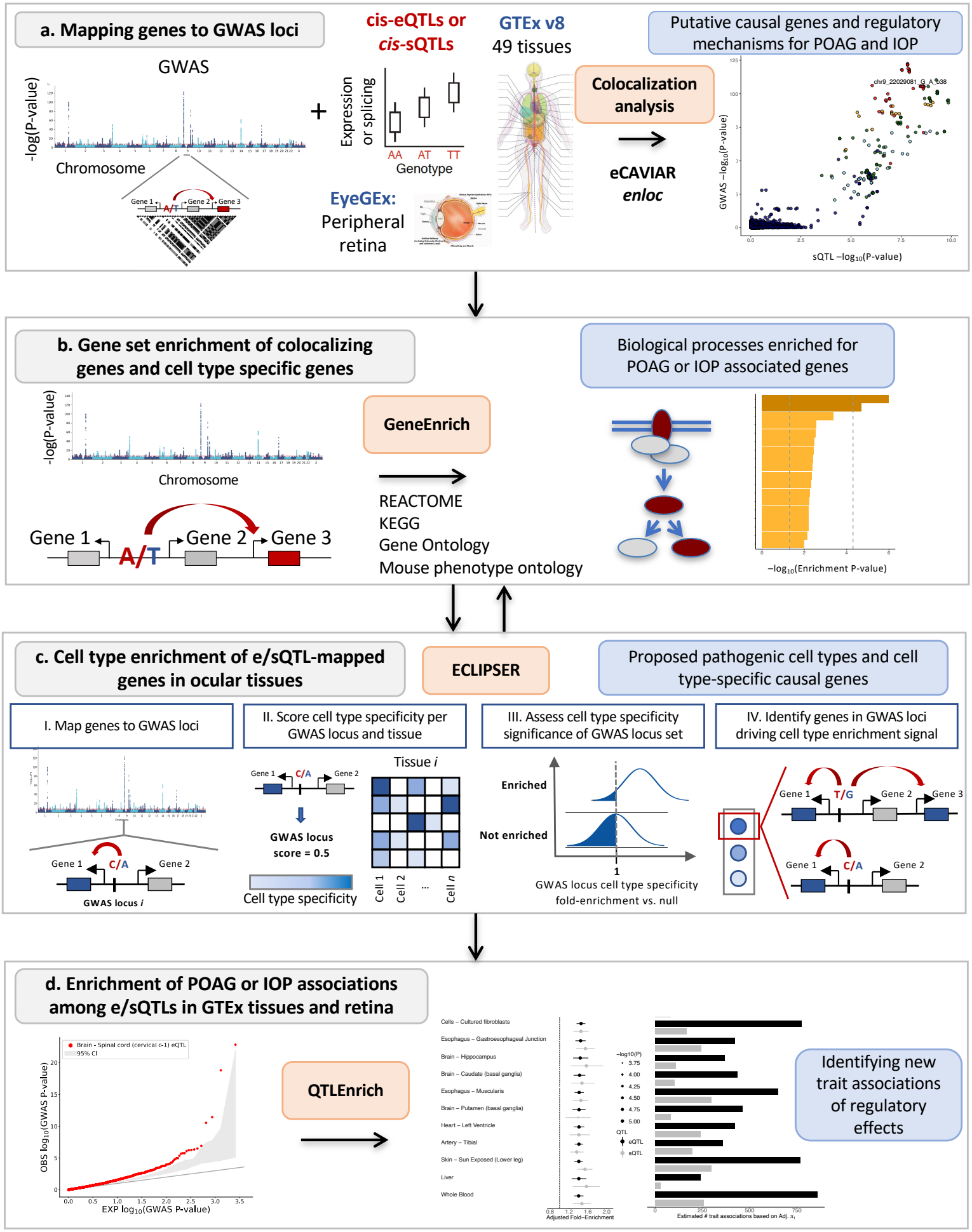
a. Mapping genes to GWAS loci
GWAS
-log(P-value)
Chromosome
Gene 1
A/T
Gene 2
Gene 3
cis-eQTLs or cis-sQTLs
Expression or splicing
AA
AT
TT
Genotype
GTEx v8
49 tissues
EyeGEx:
Peripheral retina
Colocalization analysis
eCAVIAR
enloc
Putative causal genes and regulatory mechanisms for POAG and IOP
GWAS −log10(P-value)
sQTL −log10(P-value)
b. Gene set enrichment of colocalizing genes and cell type specific genes
-log(P-value)
Chromosome
Gene 1
A/T
Gene 2
Gene 3
GeneEnrich
REACTOME
KEGG
Gene Ontology
Mouse phenotype ontology
Biological processes enriched for POAG or IOP associated genes
−log10(Enrichment P-value)
c. Cell type enrichment of e/sQTL-mapped genes in ocular tissues
ECLIPSER
Proposed pathogenic cell types and cell type-specific causal genes
I. Map genes to GWAS loci
Gene 1
C/A
Gene 2
GWAS locus i
II. Score cell type specificity per GWAS locus and tissue
Gene 1
C/A
Gene 2
GWAS locus score = 0.5
Cell type specificity
Tissue i
Cell 1
Cell 2
...
Cell n
III. Assess cell type specificity significance of GWAS locus set
Enriched
Not enriched
1
GWAS locus cell type specificity fold-enrichment vs. null
IV. Identify genes in GWAS loci driving cell type enrichment signal
Gene 1
T/G
Gene 2
Gene 3
Gene 1
C/A
Gene 2
d. Enrichment of POAG or IOP associations among e/sQTLs in GTEx tissues and retina
Brain - Spinal cord (cervical c-1) eQTL
95% CI
OBS log10(GWAS P-value)
EXP log10(GWAS P-value)
QTLEnrich
Cells – Cultured fibroblasts
Esophagus – Gastroesophageal Junction
Brain – Hippocampus
Brain – Caudate (basal ganglia)
Esophagus – Muscularis
Brain – Putamen (basal ganglia)
Heart – Left Ventricle
Artery – Tibial
Skin – Sun Exposed (Lower leg)
Liver
Whole Blood
−log10(P)
QTL
eQTL
sQTL
Adjusted Fold−Enrichment
Estimated # trait associations based on Adj. π1
Identifying new trait associations of regulatory effects

Figure 1. Analysis workflow from POAG and IOP GWAS to causal regulatory mechanisms, genes, pathways, and cell types. a, Putative causal genes were prioritized per known POAG and IOP GWAS locus by applying two colocalization methods to all e/sQTLs from 49 GTEx tissues and retina eQTLs that overlapped each locus. A Manhattan plot of the POAG cross-ancestry GWAS meta-analysis[8] was plotted with QMplot (URLs). **b**, All target genes of significantly colocalizing e/sQTLs per trait were tested for enrichment in signaling and metabolic pathways (Reactome, KEGG), gene ontologies and mouse phenotype ontologies using *GeneEnrich*. **c**, Significantly colocalizing e/sGenes were tested for enrichment in specific cell types in single nucleus RNA-seq data of glaucoma-relevant eye tissues, using ECLIPSER. A gene was considered significant with cell type fold-change >1.3 and FDR<0.1 per tissue. Cell type specificity significance per GWAS locus set for a given trait was assessed against a null distribution of GWAS loci associated with unrelated, non-ocular traits, using a Bayesian Fisher's exact test. Genes mapped to GWAS loci with a cell type specificity score above the 95th percentile of null locus scores were proposed as contributing to the trait in the enriched cell type. **d**, All POAG and IOP associations genome-wide, beyond the known GWAS loci, were tested for enrichment among e/sQTLs in GTEx tissues and retina compared to permuted null sets of variants matched on confounding factors, using *QTLEnrich*. If enrichment was found, the number of e/sQTLs in a given tissue likely to be true trait associations was estimated based on an empirically derived, true positive rate (π_1) approach.

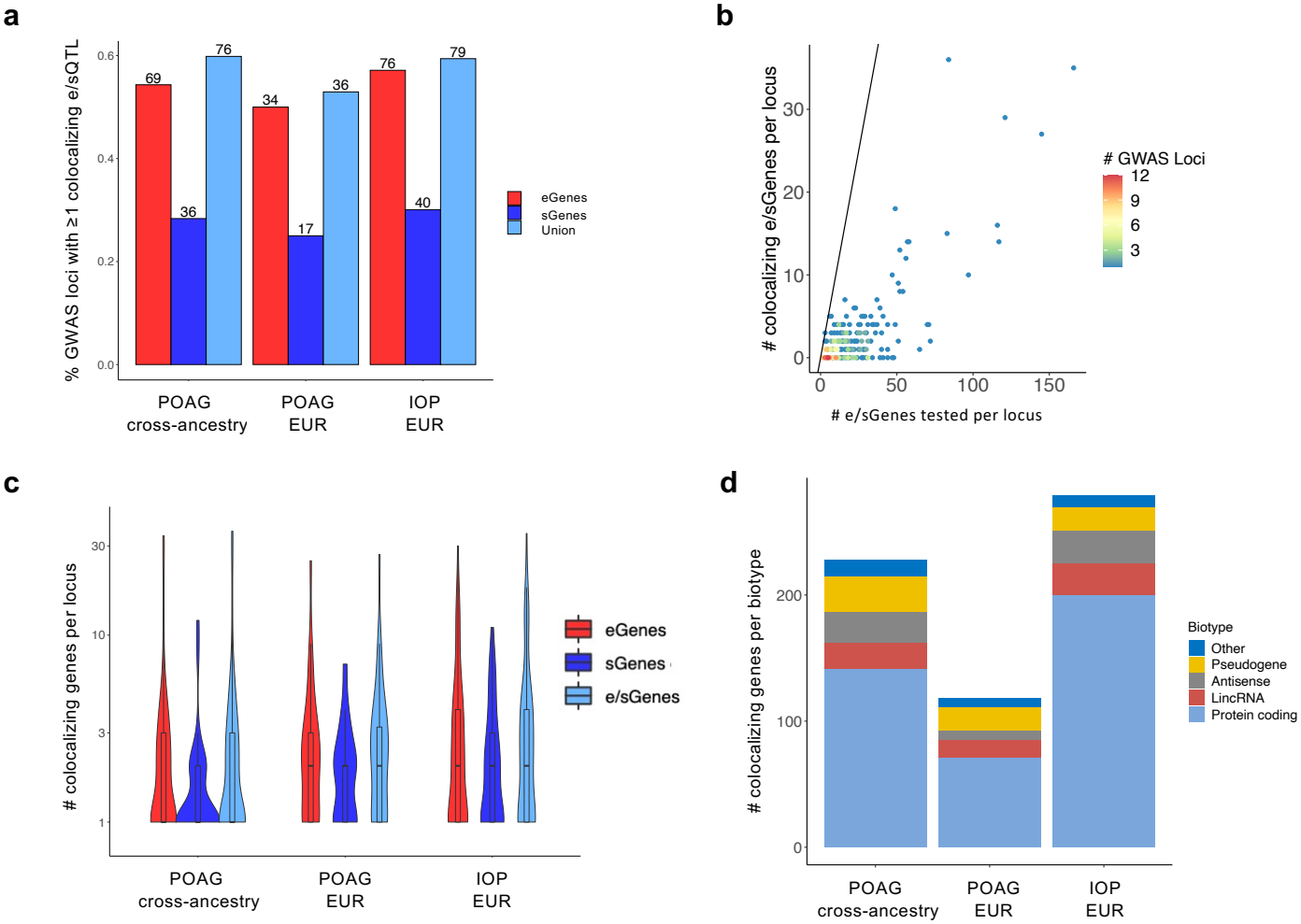

Figure 2. Summary of colocalization analysis of POAG and IOP GWAS loci with eQTLs and sQTLs. a, Histogram of percent of GWAS loci with at least one colocalizing e/sQTL (eCAVIAR CLPP > 0.01 and/or *enloc* RCP > 0.1) across the three traits (POAG Cross-ancestry, POAG European (EUR) ancestry subset, and IOP European ancestry). Numbers above the bars represent the number of loci with at least one colocalizing e/sQTL. Red, dark blue, and light blue bars indicate percentage of loci with at least one colocalizing eGene, sGene, or both, respectively. **b**, Scatter plot comparing unique number of e/sGenes per locus that significantly colocalized per locus versus unique number of e/sGenes tested per locus. Points are color-coded by number of GWAS loci. The black line represents the diagonal. **c**, Violin plots showing distribution of the unique number of colocalizing eGenes (red), sGenes (dark blue), or both (light blue) per locus for the three GWAS tested. The center line in the box plots contained within each violin plot shows the median and the box edges depict the interquartile range. **d**, Stacked histogram showing the number of colocalizing e/sGenes per gene biotype for each GWAS. Protein coding (light blue), lincRNA (brown), antisense (gray), pseudogenes (yellow), and other (dark blue).

Figure 3

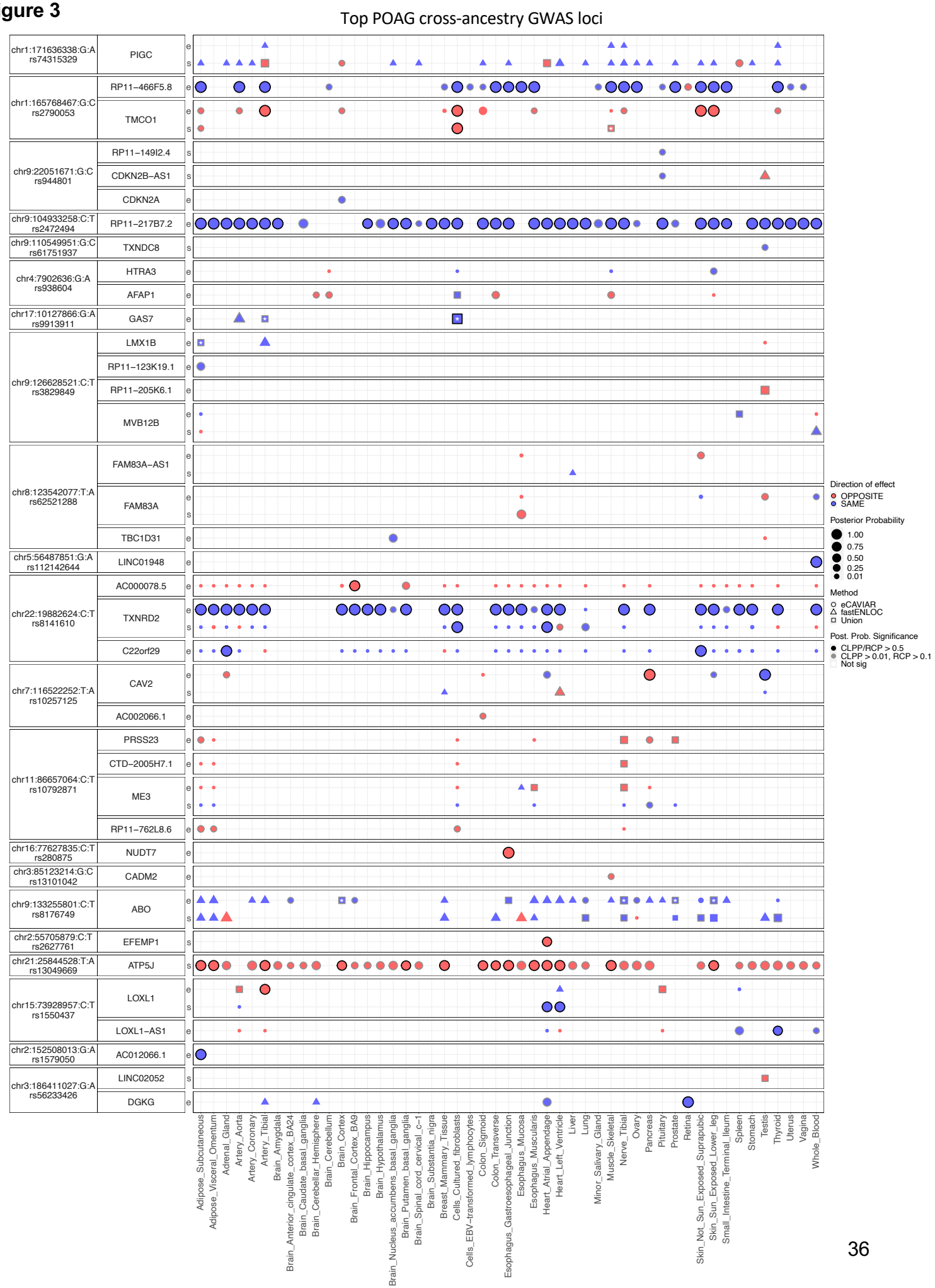
Top POAG cross-ancestry GWAS loci
chr1:171636338:G:A rs74315329
PIGC
chr1:165768467:G:C rs2790053
RP11−466F5.8
TMCO1
chr9:22051671:G:C rs944801
RP11−149I2.4
CDKN2B−AS1
CDKN2A
chr9:104933258:C:T rs2472494
RP11−217B7.2
chr9:110549951:G:C rs61751937
TXNDC8
chr4:7902636:G:A rs938604
HTRA3
AFAP1
chr17:10127866:G:A rs9913911
GAS7
chr9:126628521:C:T rs3829849
LMX1B
RP11−123K19.1
RP11−205K6.1
MVB12B
chr8:123542077:T:A rs62521288
FAM83A−AS1
FAM83A
TBC1D31
chr5:56487851:G:A rs112142644
LINC01948
chr22:19882624:C:T rs8141610
AC000078.5
TXNRD2
C22orf29
chr7:116522252:T:A rs10257125
CAV2
AC002066.1
chr11:86657064:C:T rs10792871
PRSS23
CTD−2005H7.1
ME3
RP11−762L8.6
chr16:77627835:C:T rs280875
NUDT7
chr3:85123214:G:C rs13101042
CADM2
chr9:133255801:C:T rs8176749
ABO
chr2:55705879:C:T rs2627761
EFEMP1
chr21:25844528:T:A rs13049669
ATP5J
chr15:73928957:C:T rs1550437
LOXL1
LOXL1−AS1
chr2:152508013:G:A rs1579050
AC012066.1
chr3:186411027:G:A rs56233426
LINC02052
DGKG
Adipose_Subcutaneous
Adipose_Visceral_Omentum
Adrenal_Gland
Artery_Aorta
Artery_Coronary
Artery_Tibial
Brain_Amygdala
Brain_Anterior_cingulate_cortex_BA24
Brain_Caudate_basal_ganglia
Brain_Cerebellar_Hemisphere
Brain_Cerebellum
Brain_Cortex
Brain_Frontal_Cortex_BA9
Brain_Hippocampus
Brain_Hypothalamus
Brain_Nucleus_accumbens_basal_ganglia
Brain_Putamen_basal_ganglia
Brain_Spinal_cord_cervical_c−1
Brain_Substantia_nigra
Breast_Mammary_Tissue
Cells_Cultured_fibroblasts
Cells_EBV−transformed_lymphocytes
Colon_Sigmoid
Colon_Transverse
Esophagus_Gastroesophageal_Junction
Esophagus_Mucosa
Esophagus_Muscularis
Heart_Atrial_Appendage
Heart_Left_Ventricle
Liver
Lung
Minor_Salivary_Gland
Muscle_Skeletal
Nerve_Tibial
Ovary
Pancreas
Pituitary
Prostate
Retina
Skin_Not_Sun_Exposed_Suprapubic
Skin_Sun_Exposed_Lower_leg
Small_Intestine_Terminal_Ileum
Spleen
Stomach
Testis
Thyroid
Uterus
Vagina
Whole_Blood
Direction of effect
OPPOSITE
SAME
Posterior Probability
1.00
0.75
0.50
0.25
0.01
Method
eCAVIAR
fastENLOC
Union
Post. Prob. Significance
CLPP/RCP > 0.5
CLPP > 0.01, RCP > 0.1
Not sig

Figure 3. Colocalizing e/sQTLs in GTEx tissues and retina with top POAG GWAS loci. Genes with at least one significant colocalization result are shown for e/sQTLs tested across 49 GTEx tissues and peripheral retina for the top 21 POAG cross-ancestry GWAS loci. GWAS loci were ordered by absolute value of their effect size. Within each locus, genes were ordered based on their chromosome position. Bubble size is proportional to the maximum colocalization posterior probability of all e/sVariants tested for the given gene, QTL type and tissue combination. Points are color-coded by direction of effect (blue if increased expression or splicing increases POAG risk or vice versa; red if increased expression or splicing decreases POAG risk or vice versa). Shape of points indicates colocalization method used: circle (eCAVIAR), triangle (*enloc*), and square (tested in both methods; results shown for method with maximum posterior probability). Gray or black border denotes variant-gene-tissue-QTL combination that passed QC filtering (Methods) and a colocalization posterior probability cutoff above 0.01/0.1 (CLPP/RCP) or 0.5 (higher confidence), respectively. White or black asterisk in the square indicates whether the second method tested passed a posterior probability cutoff 0.01/0.1 (CLPP/RCP) or 0.5, respectively.

Figure 4

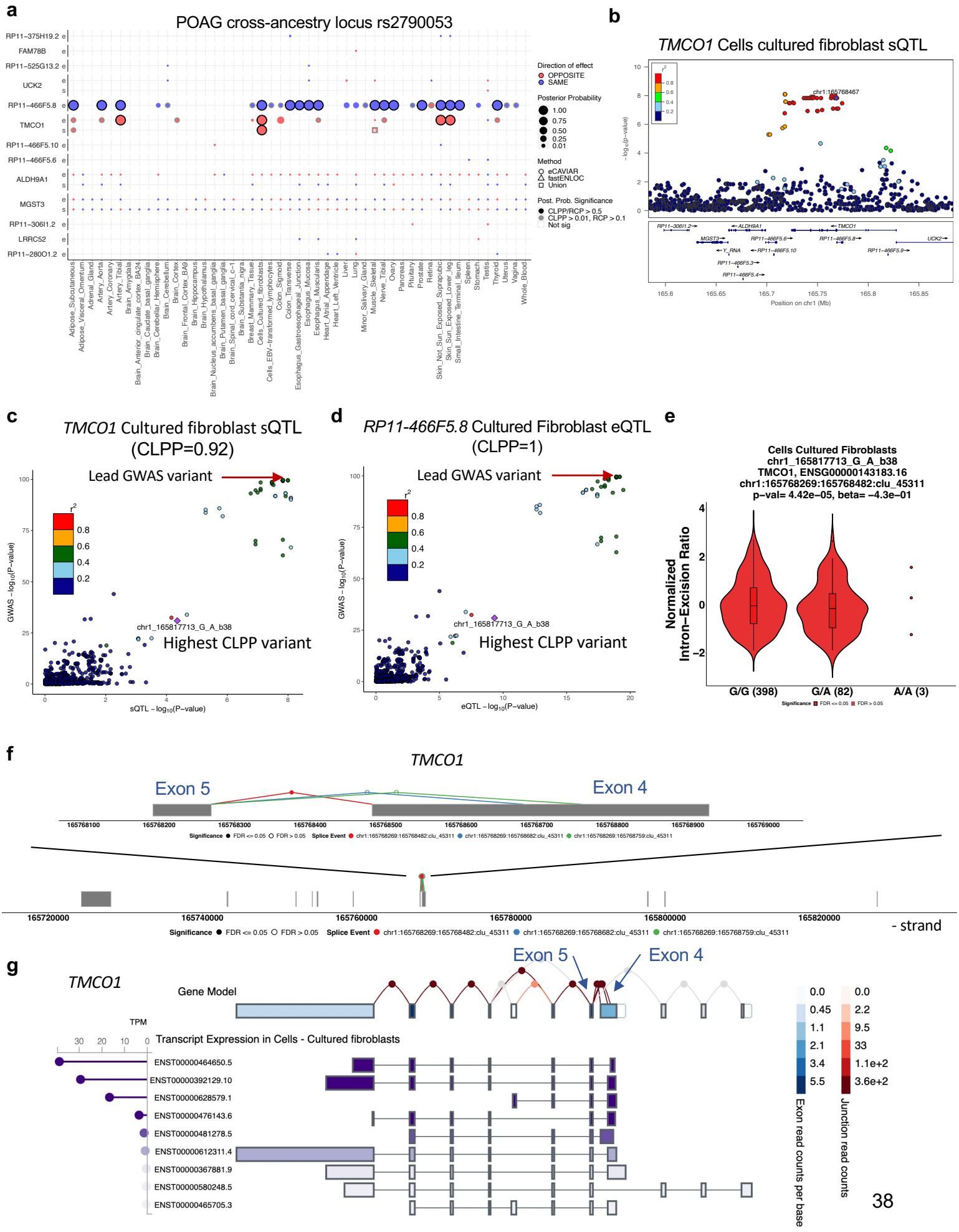
a
POAG cross-ancestry locus rs2790053
RP11−375H19.2
FAM78B
RP11−525G13.2
UCK2
RP11−466F5.8
TMCO1
RP11−466F5.10
RP11−466F5.6
ALDH9A1
MGST3
RP11−306I1.2
LRRC52
RP11−280O1.2
Direction of effect
OPPOSITE
SAME
Posterior Probability
1.00
0.75
0.50
0.25
0.01
Method
eCAVIAR
fastENLOC
Union
Post. Prob. Significance
CLPP/RCP > 0.5
CLPP > 0.01, RCP > 0.1
Not sig
b
TMCO1 Cells cultured fibroblast sQTL
chr1:165768467
Position on chr1 (Mb)
c
TMCO1 Cultured fibroblast sQTL
(CLPP=0.92)
Lead GWAS variant
chr1_165817713_G_A_b38
Highest CLPP variant
GWAS − log10(P−value)
sQTL − log10(P−value)
d
RP11-466F5.8 Cultured Fibroblast eQTL
(CLPP=1)
Lead GWAS variant
chr1_165817713_G_A_b38
Highest CLPP variant
GWAS − log10(P−value)
eQTL − log10(P−value)
e
Cells Cultured Fibroblasts
chr1_165817713_G_A_b38
TMCO1, ENSG00000143183.16
chr1:165768269:165768482:clu_45311
p−val= 4.42e−05, beta= −4.3e−01
Normalized
Intron−Excision Ratio
G/G (398)
G/A (82)
A/A (3)
f
TMCO1
Exon 5
Exon 4
Splice Event
- strand
g
TMCO1
Gene Model
Exon 5
Exon 4
TPM
Transcript Expression in Cells - Cultured fibroblasts
ENST00000464650.5
ENST00000392129.10
ENST00000628579.1
ENST00000476143.6
ENST00000481278.5
ENST00000612311.4
ENST00000367881.9
ENST00000580248.5
ENST00000465705.3
Exon read counts per base
Junction read counts

Figure 4. Examples of colocalizing e/sQTLs with top POAG and IOP GWAS loci. a, Colocalization results for all e/sGenes tested in the POAG cross-ancestry rs2790053 locus LD interval that had at least one significant eQTL or sQTL result across 49 GTEx tissues and peripheral retina based on eCAVIAR or *enloc*. Genes were ordered by chromosome position. Size of points is proportional to the maximum colocalization posterior probability of all e/sVariants tested for the given gene, QTL type and tissue combination. Points are color-coded by direction of effect (blue if increased expression or splicing increases POAG risk or vice versa; red if increased expression or splicing decreases POAG risk or vice versa). Shape of points indicates colocalization method used: circle (eCAVIAR), triangle (*enloc*), and square (tested in both methods; results shown for method with maximum posterior probability). Gray or black border denote variant-gene-tissue-QTL combination that passed QC filtering (Methods) and a colocalization posterior probability cutoff above 0.01/0.1 (CLPP/RCP) or 0.5, respectively. White or black asterisk in the square indicates whether the second method tested passed a posterior probability cutoff of 0.01/0.1 (CLPP/RCP) or 0.5, respectively. **b**, LocusZoom[83] plot for *TMCO1* sQTL -$\log_{10}$(P-value) in GTEx Cells Cultured fibroblasts in the POAG cross-ancestry GWAS variant rs2790053 (chr1_165768467_C_G_b38) LD interval. Points are color-coded by LD (r^2) relative to the lead GWAS variant, chr1_165768467_C_G_b38. **c**,**d** LocusCompare plot of -$\log_{10}$(P-value) of the POAG cross-ancestry GWAS meta-analysis versus the -$\log_{10}$(P-value) of the Cells Cultured fibroblast sQTL or eQTL acting on *TMCO1* (**c**) or *RP11-466F5.8* (**d**), respectively. Points are color-coded based on LD (r^2) relative to the variant with the highest eCAVIAR colocalization posterior probability (CLPP). **e,** Violin plot of normalized intron-excision ratio for chr1:165768269-165768482 computed with Leafcutter[82] for *TMCO1* in Cells Cultured fibroblasts as a function of the genotype of the sVariant chr1_165817713_G_A_b38 (rs143863391) with the highest CLPP (0.92) for this sQTL and the POAG cross-ancestry GWAS locus rs2790053. The effect size of the sQTL relative to the alternative allele (*beta* = -0.43) is in opposite direction relative to the GWAS variant (*beta* = 0.25), suggesting that decreased splicing between chr1:165768269-165768482 increases POAG risk. **f,** Gene model for *TMCO1* in GTEx Cells Cultured fibroblasts on the negative strand showing all the intron excision splicing events detected with Leafcutter in *TMCO1*. A zoom in of the splicing event (chr1:165768269-165768482; red), an alternative splice donor site on exon 4 (red versus blue or green), associated with an sVariant (chr1_165817713_G_A_b38) that colocalized with POAG risk is shown. A longer exon 4 in *TMCO1* is associated with decreased risk of POAG. **g,** *TMCO1* gene model and transcripts expressed in Cells Cultured fibroblasts taken from the GTEx portal (URLs). In the gene model, exon boxes are color-coded by exon read counts per base (blue) and lines connecting exons by exon-exon junction read counts (red). All splicing events observed in the tissue are shown, including the alternative splice event between exon 4 and exon 5 whose genetic regulation colocalized with POAG (**c**). Below the gene model, transcript expression in Cells Cultured fibroblasts in Transcripts per Million (TPM), computed with RSEM[93], is shown in descending order.

Figure 5

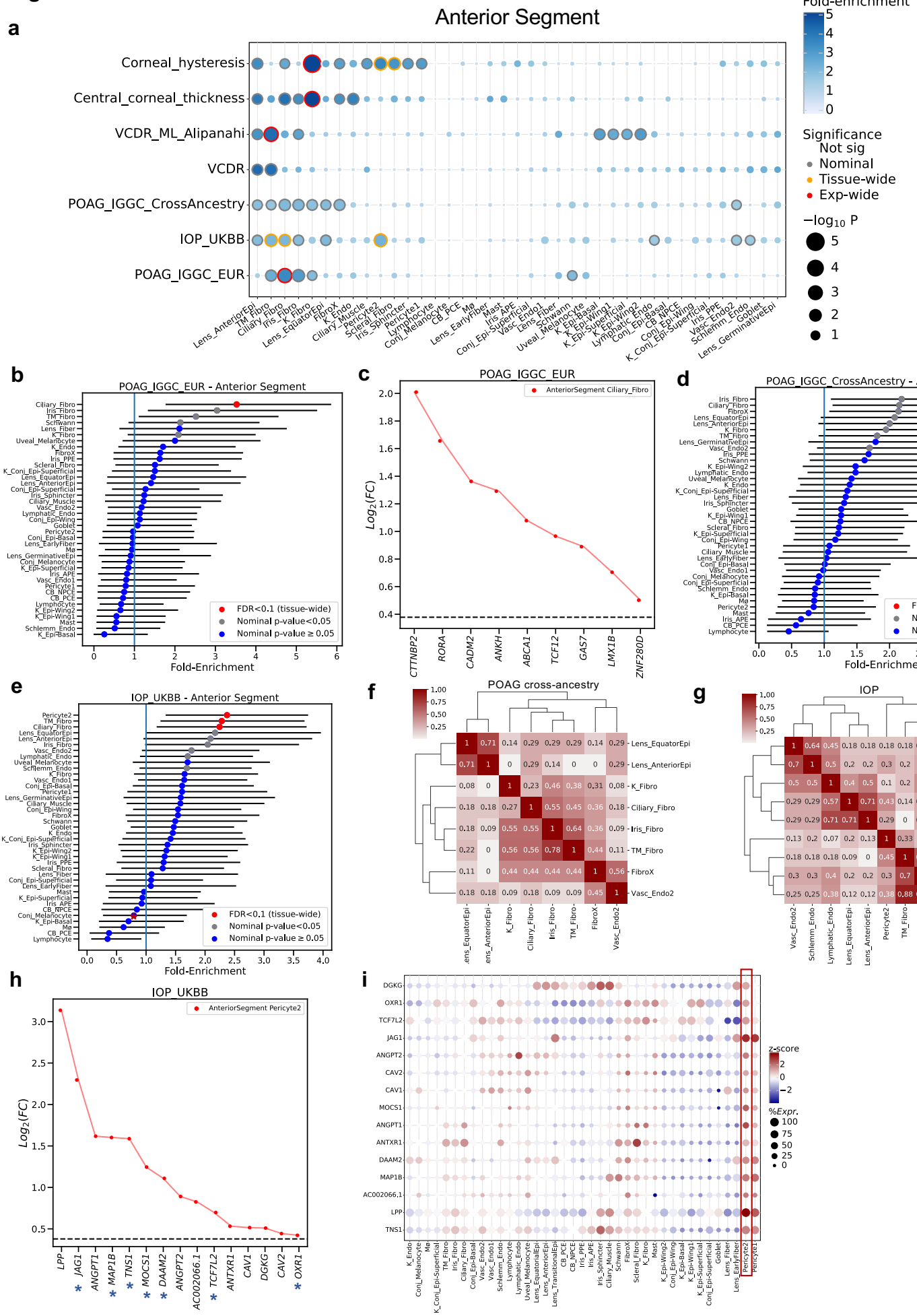
a
Anterior Segment
Corneal_hysteresis
Central_corneal_thickness
VCDR_ML_Alipanahi
VCDR
POAG_IGGC_CrossAncestry
IOP_UKBB
POAG_IGGC_EUR
Fold-enrichment
Significance
Not sig
Nominal
Tissue-wide
Exp-wide
−log10 P
b
POAG_IGGC_EUR - Anterior Segment
FDR<0.1 (tissue-wide)
Nominal p-value<0.05
Nominal p-value ≥ 0.05
Fold-Enrichment
c
POAG_IGGC_EUR
AnteriorSegment Ciliary_Fibro
Log2(FC)
CTTNBP2
RORA
CADM2
ANKH
ABCA1
TCF12
GAS7
LMX1B
ZNF280D
d
POAG_IGGC_CrossAncestry - Anterior Segment
FDR<0.1 (tissue-wide)
Nominal p-value<0.05
Nominal p-value ≥ 0.05
Fold-Enrichment
e
IOP_UKBB - Anterior Segment
FDR<0.1 (tissue-wide)
Nominal p-value<0.05
Nominal p-value ≥ 0.05
Fold-Enrichment
f
POAG cross-ancestry
g
IOP
h
IOP_UKBB
AnteriorSegment Pericyte2
Log2(FC)
LPP
JAG1
ANGPT1
MAP1B
TNS1
MOCS1
DAAM2
ANGPT2
AC002066.1
TCF7L2
ANTXR1
CAV1
DGKG
CAV2
OXR1
i
DGKG
OXR1
TCF7L2
JAG1
ANGPT2
CAV2
CAV1
MOCS1
ANGPT1
ANTXR1
DAAM2
MAP1B
AC002066.1
LPP
TNS1
z-score
%Expr.

Figure 5. Cell type enrichment of e/sQTL-mapped genes for POAG, IOP and related trait loci in the anterior segment of the eye. a, Significance (circle size, -log10(P-value)) and fold-enrichment (circle color) of the cell type specificity of GWAS locus sets for POAG cross-ancestry, POAR European subset, IOP, central cornea thickness, corneal hysteresis, physician-defined Vertical-cup-to-disc ratio (VCDR), and machine learning (ML)-defined VCDR (VCDR_ML_Alipanahi) are shown for each of the 39 cell types found in six tissues in the anterior segment of the eye[28]. Traits (rows) and cell types (columns) were clustered based on hierarchical clustering of the euclidean distance between GWAS locus set cell type-specificity enrichment scores. Red rings: experiment-wide significant (Benjamini Hochberg (BH) FDR<0.1); Yellow rings: tissue-wide significant (BH FDR<0.1); Gray rings: nominal significant (P<0.05). **b,d,e** Cell type specificity fold-enrichment (x-axis) in the different anterior segment cell types ranked in descending order for the POAG European subset (**b**), POAG cross-ancestry (**d**), and IOP (**e**) GWAS locus sets. Error bars: 95% confidence intervals. Red: tissue-wide significant (FDR<0.1); Gray: nominal significant (P<0.05); Blue: non-significant (P≥0.05). **c,h,** Differential expression ($\log_2$(Fold-change), y axis) in the most strongly enriched cell type compared to all other cell types is shown for the set of genes (x axis) driving the enrichment signal of the POAG European GWAS loci in ciliary fibroblasts (**c**) and the IOP GWAS loci in pericytes (cluster 2) (**h**). Vertical dashed line represents $\log_2$(Fold-change) of 0.375 (FC=1.3) and FDR<0.1 that was used as the cell type-specificity enrichment cutoff. Asterisks denote genes in IOP loci not associated with POAG risk (**h**). **f-g**, Heatmap of fraction of genes that overlap between the e/sGenes driving the enrichment signal for top ranked cell types (P<0.05) in the anterior segment for POAG cross-ancestry (CA) (**f**) and IOP (**g**) GWAS loci. Numbers refer to the fraction of e/sGenes driving the cell type enrichment on each row that overlaps with the genes driving the cell type enrichment on the corresponding column. Hierarchical clustering was performed on both rows and columns using the euclidean distance between fractions. Red asterisks: tissue-wide BH FDR<0.1. **i,** Bubble map displaying the expression of the e/sGenes driving the IOP enrichment in pericytes across all cell types in the anterior segment. The colorbar represents gene expression z-scores computed by comparing each gene's average expression in a given cell type to its per cell type average expression across all types divided by the standard deviation of all cell type expression averages. Bubble size is proportional to the percentage of cells expressing the given gene (log(TPK+1)>1). Cell type abbreviations are described in Supplementary Table 31.

Figure 6

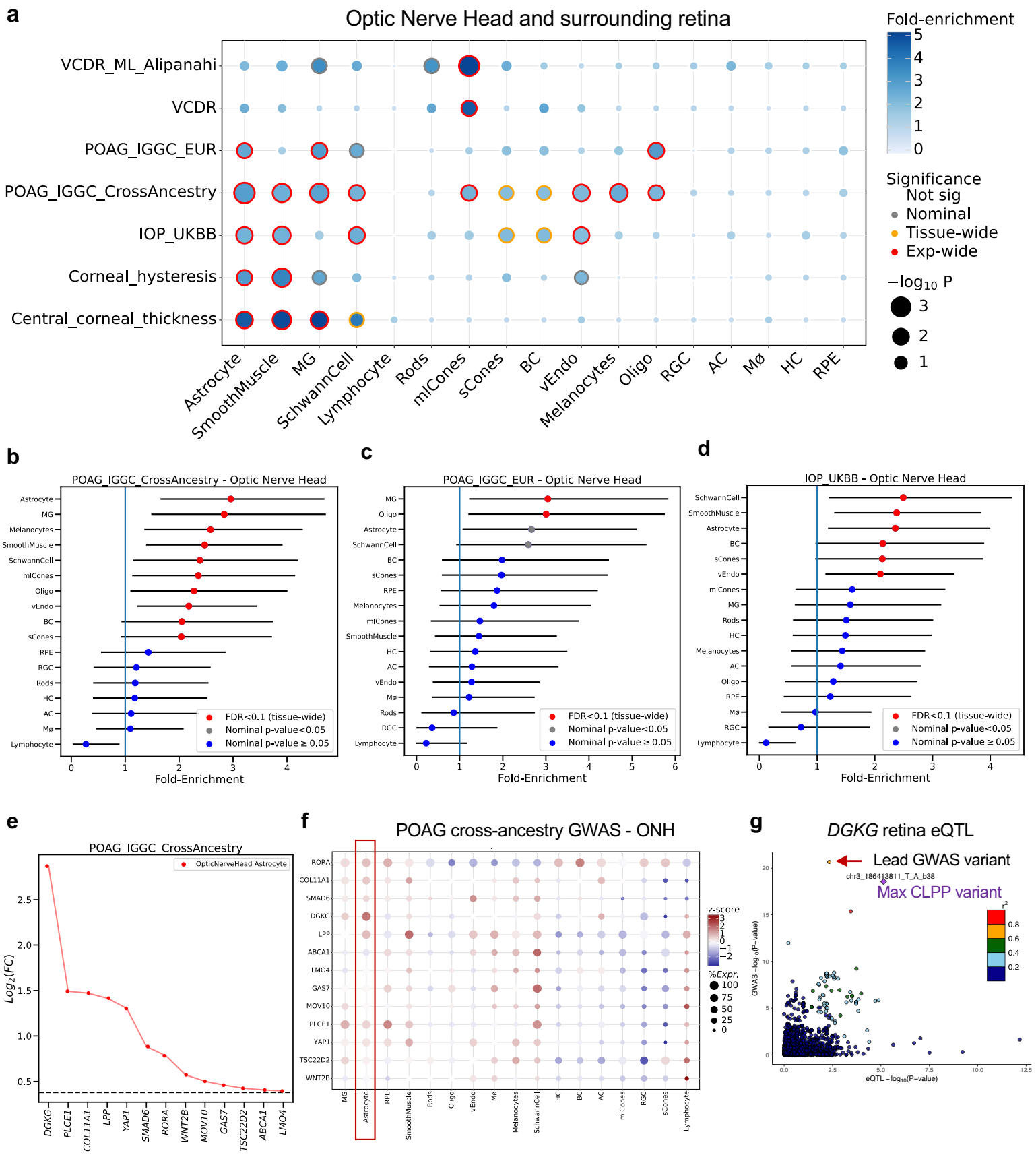
a
Optic Nerve Head and surrounding retina
VCDR_ML_Alipanahi
VCDR
POAG_IGGC_EUR
POAG_IGGC_CrossAncestry
IOP_UKBB
Corneal_hysteresis
Central_corneal_thickness
Astrocyte
SmoothMuscle
MG
SchwannCell
Lymphocyte
Rods
mlCones
sCones
BC
vEndo
Melanocytes
Oligo
RGC
AC
Mø
HC
RPE
Fold-enrichment
Significance
Not sig
Nominal
Tissue-wide
Exp-wide
−log10 P
b
POAG_IGGC_CrossAncestry - Optic Nerve Head
FDR<0.1 (tissue-wide)
Nominal p-value<0.05
Nominal p-value ≥ 0.05
Fold-Enrichment
c
POAG_IGGC_EUR - Optic Nerve Head
d
IOP_UKBB - Optic Nerve Head
e
POAG_IGGC_CrossAncestry
OpticNerveHead Astrocyte
Log2(FC)
f
POAG cross-ancestry GWAS - ONH
RORA
COL11A1
SMAD6
DGKG
LPP
ABCA1
LMO4
GAS7
MOV10
PLCE1
YAP1
TSC22D2
WNT2B
z-score
%Expr.
g
DGKG retina eQTL
Lead GWAS variant
chr3_186413811_T_A_b38
Max CLPP variant
GWAS −log10(P-value)
eQTL −log10(P-value)

Figure 6. Cell type enrichment of e/sQTL-mapped genes for POAG, IOP and related trait loci in optic nerve head and surrounding retina. a, Significance (circle size, -log10(P-value)) and fold-enrichment (circle color) of the cell type specificity of GWAS locus sets for POAG cross-ancestry, POAR European subset, IOP, central cornea thickness, corneal hysteresis, and physician (VCDR) and machine learning (ML)-defined VCDR (VCDR_ML_Alipanahi) are shown for each of the 17 cell types found in optic nerve head (ONH) and surrounding retina. Traits (rows) and cell types (columns) were clustered based on hierarchical clustering of the euclidean distance between GWAS locus set cell type-specificity enrichment scores. Red rings: experiment-wide significant (Benjamini Hochberg (BH) FDR<0.1); Yellow rings: tissue-wide significant (BH FDR<0.1); Gray rings: nominal significant (P<0.05). **b-d,** Cell type specificity fold-enrichment (x-axis) in the ONH cell types ranked in descending order for the POAG cross-ancestry (**b**), POAG European (**c**), and IOP (**d**) GWAS locus sets. **e,** Differential expression (log_2(Fold-change)) in astrocytes, the most strongly enriched cell type for POAG cross-ancestry GWAS loci in the ONH, compared to all other cell types is shown for the set of genes driving the POAG enrichment signal in astrocytes. Vertical dashed line represents log_2(Fold-change) of 0.375 (FC=1.3) and FDR<0.1 that was used as the cell type-specificity enrichment cutoff. **f,** The expression profile of the e/sGenes driving the POAG cross-ancestry enrichment signal in astrocytes is shown across all cell types in the optic nerve head (ONH). Color represents z-scores computed by comparing each gene's average expression in a given cell type to the average expression across cell types divided by its standard deviation of all cell type expression averages. Bubble size is proportional to the percentage of cells expressing the gene (log(TPK+1)>1). **g,** LocusCompare plot of -log_{10} (P-value) of the POAG cross-ancestry GWAS meta-analysis relative to -log_{10}(P-value) of a retina eQTL acting on *DGKG* that significantly colocalized with the POAG GWAS locus rs56233426 (chr3_186411027_G_A). *DGKG* is the strongest astrocyte-specific gene driving the cell type enrichment signal for POAG loci. Points are color-coded based on LD (r^2) relative to the eVariant with the highest colocalization posterior probability (CLPP=0.93). The red arrow is pointing to the lead POAG GWAS variant. MG, Müller Glia; BC, bipolar cells; vEndo, vascular endothelium; Oligo, oligodendrocytes; RGC, retinal ganglion cells; AC, amacrine cells; Mø, macrophages; HC, horizontal cells; RPE, retinal pigment epithelium.

Figure 7

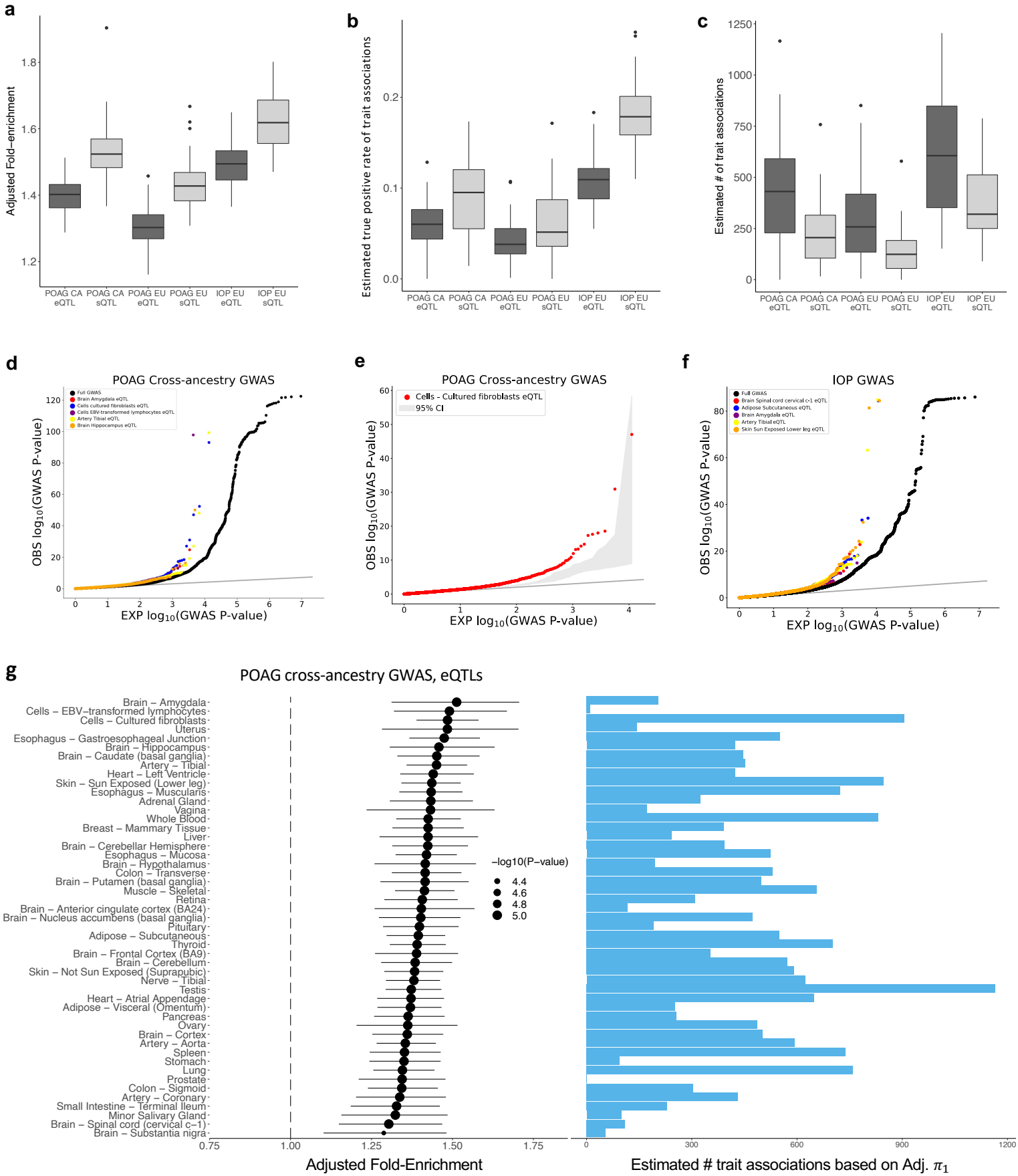
a
Adjusted Fold−enrichment
POAG CA eQTL
POAG CA sQTL
POAG EU eQTL
POAG EU sQTL
IOP EU eQTL
IOP EU sQTL
b
Estimated true positive rate of trait associations
c
Estimated # of trait associations
d
POAG Cross-ancestry GWAS
Full GWAS
Brain Amygdala eQTL
Cells cultured fibroblasts eQTL
Cells EBV-transformed lymphocytes eQTL
Artery Tibial eQTL
Brain Hippocampus eQTL
OBS log10(GWAS P-value)
EXP log10(GWAS P-value)
e
POAG Cross-ancestry GWAS
Cells - Cultured fibroblasts eQTL
95% CI
OBS log10(GWAS P-value)
EXP log10(GWAS P-value)
f
IOP GWAS
Full GWAS
Brain Spinal cord cervical c-1 eQTL
Adipose Subcutaneous eQTL
Brain Amygdala eQTL
Artery Tibial eQTL
Skin Sun Exposed Lower leg eQTL
OBS log10(GWAS P-value)
EXP log10(GWAS P-value)
g
POAG cross-ancestry GWAS, eQTLs
Brain – Amygdala
Cells – EBV−transformed lymphocytes
Cells – Cultured fibroblasts
Uterus
Esophagus – Gastroesophageal Junction
Brain – Hippocampus
Brain – Caudate (basal ganglia)
Artery – Tibial
Heart – Left Ventricle
Skin – Sun Exposed (Lower leg)
Esophagus – Muscularis
Adrenal Gland
Vagina
Whole Blood
Breast – Mammary Tissue
Liver
Brain – Cerebellar Hemisphere
Esophagus – Mucosa
Brain – Hypothalamus
Colon – Transverse
Brain – Putamen (basal ganglia)
Muscle – Skeletal
Retina
Brain – Anterior cingulate cortex (BA24)
Brain – Nucleus accumbens (basal ganglia)
Pituitary
Adipose – Subcutaneous
Thyroid
Brain – Frontal Cortex (BA9)
Brain – Cerebellum
Skin – Not Sun Exposed (Suprapubic)
Nerve – Tibial
Testis
Heart – Atrial Appendage
Adipose – Visceral (Omentum)
Pancreas
Ovary
Brain – Cortex
Artery – Aorta
Spleen
Stomach
Lung
Prostate
Colon – Sigmoid
Artery – Coronary
Small Intestine – Terminal Ileum
Minor Salivary Gland
Brain – Spinal cord (cervical c−1)
Brain – Substantia nigra
−log10(P−value)
4.4
4.6
4.8
5.0
Adjusted Fold-Enrichment
Estimated # trait associations based on Adj. π_1

Figure 7. e/sQTLs enriched for hundreds of new POAG and IOP associations. a-c, Boxplots showing the distributions of three *QTLEnrich* summary statistics for POAG Cross-ancestry GWAS, POAG European (EUR) ancestry GWAS, and IOP GWAS for the significant tissue-trait pairs that passed Bonferroni correction for testing enrichment of trait associations amongst eQTLs (dark gray) and sQTLs (light gray) from 49 GTEx tissues and retina eQTLs: adjusted fold-enrichment (**a**), estimated true positive rate of trait associations among e/sQTLs (Adjusted $\boldsymbol{\pi}_1$) (**b**), and estimated number of trait associations based on adjusted $\boldsymbol{\pi}_1$ **(c)**. The center lines in the box plots depict the median value and the box edges the interquartile range. **d**, **f** Quantile-quantile (Q-Q) plot of POAG Cross-ancestry (**d**) and IOP (**f**) GWAS -$\log_{10}$ (P-value) compared to expectation for the best eQTL per eGene set (eVariants with FDR < 0.05) of the top enriched tissues based on adjusted fold-enrichment (colored lines), compared to all variants in the GWAS (black points). Gray line represents the diagonal. **e**, Q-Q plot of POAG Cross-ancestry GWAS -$\log_{10}$(P-value) for the significant best eQTL per eGene set (FDR < 0.05) in one of the top enriched tissues, Cells - Cultured fibroblasts (red points), compared to GWAS p-values of 1,000 confounder-matched null variant sets (light gray) generated by *QTLEnrich*. **g**, Forest plots (left panel) and barplots (right panel) of all tissues whose eQTLs were significantly enriched (Bonferroni correction) for POAG Cross-ancestry GWAS associations based on *QTLEnrich*. Points indicate the adjusted fold-enrichment scaled by -log10(Enrichment P-value) and the lines represent 95% confidence intervals. Barplots show estimated number of e/sQTLs that are likely true trait associations per enriched tissue using an adjusted true positive rate, $\boldsymbol{\pi}_1$ approach. The lack of estimated number of POAG associations among prostate eQTLs is likely due to deflation of the GWAS p-values of the prostate eQTL set (see Methods).

1102 **Table 1. List of high confidence colocalizing e/sGenes with POAG and IOP GWAS loci.**

GWAS locus	RS ID	GWAS effect (OR or beta)	# e/sGenes tested per locus	# significantly colocalizing e/sGenes with eCAVIAR or enloc	Colocalizing e/sGenes with eCAVIAR and *enloc*	Significantly colocalizing Retina eQTL	Nearest Gene	Significant in GWAS:	
POAG cross-ancestry GWAS								**IOP**	**POAG European**
chr1:171636338:G:A	rs74315329	5.46957	24	1	*PIGC (s)*	-	-	-	-
chr1:165768467:G:C	rs2790053	1.35026	13	2	*TMCO1 (e,s)*	-	+	*TMCO1*	*TMCO1*
chr9:22051671:G:C	rs944801	1.2663	26	3	*CDKN2B-AS1 (s)*	-	+	-	*CDKN2B-AS1*
chr4:7902636:G:A	rs938604	0.866407	27	2	*AFAP1 (e)*	-	+	*AFAP1*	-
chr17:10127866:G:A	rs9913911	1.14912	30	1	*GAS7 (e)*	-	+	*GAS7*	*GAS7*
chr9:126628521:C:T	rs3829849	0.87529	11	4	*LMX1B (e)*	-	+	*LMX1B*	*LMX1B*
chr7:116522252:T:A	rs10257125	0.890921	18	2	*CAV2 (e,s)*	-	-	*CAV2*	*CAV2*
chr11:86657064:C:T	rs10792871	1.12142	15	4	*PRSS23 (e), ME3 (e)*	-	+	*PRSS23, ME3*	*PRSS23, ME3*
chr9:133255801:C:T	rs8176749	1.10186	18	1	*ABO (e)*	-	+	*ABO*	-
chr15:73928957:C:T	rs1550437	0.913657	72	2	*LOXL1 (e,s)*	-	+	-	*LOXL1*
chr3:188349165:G:T	rs6787621	0.92626	7	1	*LPP (e,s)*	-	+	*LPP*	-
chr22:28712241:G:A	rs5752776	0.926631	27	5	*TTC28 (e), CHEK2 (e)*	-	+	-	*TTC28, CHEK2*
chr2:12811195:C:T	rs12623251	0.932021	11	1	*TRIB2 (e)*	-	+	-	*TRIB2*
chr15:57261634:T:A	rs2431023	1.07026	16	2	*ZNF280D (e), TCF12 (e)*	-	+	-	*ZNF280D, TCF12*
chr11:130412183:C:T	rs2875238	0.935289	7	2	*RP11-121M22.1 (e,s), ADAMTS8 (e)*	-	+	-	-
chr1:53658200:G:T	rs941125	1.0646	13	2	*GLIS1 (e)*	-	+	-	-
chr7:134835770:C:A	rs10237321	0.94535	29	1	*CALD1 (e)*	-	+	-	-
chr6:134051012:G:C	rs2811688	0.946296	3	3	*SLC2A12 (e), TBPL1 (e)*	*SLC2A12*	+	-	*SLC2A12, TBPL1*
IOP GWAS								**POAG European**	**POAG cross-ancestry**
chr1:165715441:C:T	rs116089225	-0.744	29	3	*TMCO1 (e)*	-	+	*TMCO1*	*TMCO1*
chr14:74498200:C:T	rs74384554	0.417	70	4	*NPC2 (e)*	*NPC2*	-	-	*NPC2*
chr1:165745179:C:T	rs10918274	0.377	14	3	*TMCO1 (e)*	-	+	*TMCO1*	*TMCO1*
chr17:10127866:G:A	rs9913911	0.231	3	1	*GAS7 (e)*	-	+	*GAS7*	*GAS7*
chr7:116511284:C:T	rs10281637	-0.225	13	3	*CAV2 (e), CAV1 (e)*	-	+	*CAV2*	*CAV2*
chr11:120422429:G:A	rs11217863	-0.224	17	2	*ARHGEF12 (e,s)*	-	+	*ARHGEF12*	*ARHGEF12*
chr1:218937686:C:A	rs73103335	0.206	11	2	*LYPLAL1-AS1 (e,s)*	-	+	-	-
chr5:108710999:G:A	rs73220177	0.165	9	2	*LINC01023 (e)*	-	-	-	-
chr22:19854787:G:A	rs17534001	0.16	26	4	*TXNRD2 (e,s)*	-	+	*TXNRD2*	*TXNRD2*
chr6:170146547:G:T	rs59020521	-0.148	18	2	*RP11-302L19.3 (e)*	-	-	-	*RP11-302L19.3*
chr22:29224336:C:A	rs9608740	-0.141	40	3	*EMID1 (e,s)*	-	+	*EMID1*	-
chr2:238402728:C:T	rs57435966	0.132	25	3	*TRAF3IP1 (e)*	-	+	-	-
chr11:16989629:C:A	rs4141194	-0.131	18	5	*NCR3LG1 (e), KCNJ11 (e,s), NUCB2 (s)*	*NCR3LG1*	-	-	*NUCB2*
chr11:86699199:C:T	rs2433414	-0.128	22	6	*ME3 (e)*	-	+	*ME3*	*ME3*
chr11:47253513:G:A	rs10838681	-0.124	56	12	*PTPRJ (e)*	-	-	-	-
chr3:50162314:G:A	rs11710277	-0.12	117	14	*LSMEM2 (e)*	-	-	-	-
chr15:61659036:C:T	rs4775427	-0.111	7	5	*RP11-507B12.1 (e), RP11-507B12.2 (e), RP11-162I7.1 (e)*	-	-	*RP11-507B12.1, RP11-507B12.2, RP11-162I7.1*	*RP11-507B12.1, RP11-507B12.2, RP11-162I7.1*
chr14:52920118:G:C	rs8009633	0.11	12	2	*FERMT2 (e,s)*	-	+	-	-
chr2:101031432:G:A	rs55771809	0.109	17	3	*TBC1D8 (s)*	*TBC1D8*	+	-	-
chr7:116171382:C:A	rs2896175	0.108	12	4	*TES (e)*	-	-	-	-
chr16:89752083:C:T	rs3743860	0.102	57	14	*ZNF276 (e,s), SPIRE2 (e), FANCA (e,s), DPEP1 (e), VPS9D1 (e)*	-	+	-	-
chr11:78374959:C:T	rs10793308	0.098	25	4	*NARS2 (e,s), USP35 (e)*	-	-	-	-
chr11:86789159:C:T	rs11606902	-0.098	12	4	*PRSS23 (e), ME3 (e)*	*PRSS23*	+	*PRSS23, ME3*	*PRSS23, ME3*
chr1:112639117:G:C	rs61818802	-0.097	14	4	*MOV10 (e), RHOC (e)*	-	-	-	*MOV10*
chr3:50143702:G:T	rs2526385	0.096	116	16	*LSMEM2 (e)*	-	-	-	-
chr22:37788844:C:T	rs6000889	0.094	47	10	*GCAT (e,s), ANKRD54 (e)*	-	-	-	*GCAT*
chr7:11644065:C:T	rs1635182	-0.094	4	1	*THSD7A (e)*	-	+	-	*THSD7A*
chr3:188343926:C:T	rs4132172	0.093	4	2	*LPP (e,s)*	-	+		*LPP*
chr17:46758936:C:T	rs9912530	0.091	58	14	*WNT3 (e)*	-	+	*WNT3*	-
chr1:37627051:C:T	rs4074961	-0.089	17	5	*GNL2 (e,s), MEAF6 (e), DNALI1 (s)*	-	-	*GNL2, MEAF6, DNALI1*	
chr10:80411803:C:T	rs6585986	-0.084	37	4	*TSPAN14 (s), ANXA11 (e)*	-	-	-	-
chr13:75683130:G:C	rs9544022	-0.081	9	2	*LMO7 (s)*	-	+	*LMO7*	-
chr2:217802649:T:A	rs3791979	-0.081	9	2	*TNS1 (e,s)*	-	+	-	-
chr11:817786:C:T	rs10902223	0.079	49	18	*PIDD1, CRACR2B, PNPLA2, CHID1*	-	-	-	-
chr10:92670768:G:A	rs9419741	-0.077	19	4	*HHEX (e)*	-	+	-	-
chr1:31726197:G:C	rs945211	-0.073	28	5	*COL16A1 (e,s)*	-	-	-	-
chr6:39895441:G:A	rs3004063	0.071	9	3	*MOCS1 (e), RP11-61I13.3 (e,s),*	-	+	-	-
chr17:49264218:C:T	rs9899665	-0.069	31	2	*GNGT2 (e)*	-	-	-	-

1103

1104

1105 **References**

1106 1. Tham, Y.-C. *et al.* Global prevalence of glaucoma and projections of glaucoma burden
1107 through 2040: a systematic review and meta-analysis. *Ophthalmology* **121**, 2081–2090 (2014).
1108 2. Weinreb, R. N. *et al.* Primary open-angle glaucoma. *Nat Rev Dis Primers* **2**, 16067 (2016).
1109 3. Leske, M. C. *et al.* Predictors of long-term progression in the early manifest glaucoma
1110 trial. *Ophthalmology* **114**, 1965–1972 (2007).
1111 4. Kwon, Y. H., Fingert, J. H., Kuehn, M. H. & Alward, W. L. M. Primary open-angle
1112 glaucoma. *N. Engl. J. Med.* **360**, 1113–1124 (2009).
1113 5. Kim, J. *et al.* Impaired angiopoietin/Tie2 signaling compromises Schlemm's canal integrity
1114 and induces glaucoma. *J. Clin. Invest.* **127**, 3877–3896 (2017).
1115 6. Costagliola, C. *et al.* How many aqueous humor outflow pathways are there? *Surv.*
1116 *Ophthalmol.* **65**, 144–170 (2020).
1117 7. Anderson, D. R., Drance, S. M., Schulzer, M. & Collaborative Normal-Tension Glaucoma
1118 Study Group. Natural history of normal-tension glaucoma. *Ophthalmology* **108**, 247–253 (2001).
1119 8. Gharahkhani, P. *et al.* Genome-wide meta-analysis identifies 127 open-angle glaucoma
1120 loci with consistent effect across ancestries. *Nat. Commun.* **12**, 1258 (2021).
1121 9. Khawaja, A. P. *et al.* Genome-wide analyses identify 68 new loci associated with
1122 intraocular pressure and improve risk prediction for primary open-angle glaucoma. *Nature*
1123 *Genetics* vol. 50 778–782 (2018).
1124 10. MacGregor, S. *et al.* Genome-wide association study of intraocular pressure uncovers
1125 new pathways to glaucoma. *Nature Genetics* vol. 50 1067–1071 (2018).
1126 11. Gao, X. R. *et al.* Genome-wide association analyses identify new loci influencing
1127 intraocular pressure. *Human Molecular Genetics* vol. 27 2205–2213 (2018).
1128 12. Alipanahi, B. *et al.* Large-scale machine-learning-based phenotyping significantly
1129 improves genomic discovery for optic nerve head morphology. *Am. J. Hum. Genet.* **108**, 1217–
1130 1230 (2021).
1131 13. Springelkamp, H. *et al.* New insights into the genetics of primary open-angle glaucoma
1132 based on meta-analyses of intraocular pressure and optic disc characteristics. *Hum. Mol. Genet.*
1133 **26**, 438–453 (2017).
1134 14. Lu, Y. *et al.* Common genetic variants near the Brittle Cornea Syndrome locus ZNF469
1135 influence the blinding disease risk factor central corneal thickness. *PLoS Genet.* **6**, e1000947
1136 (2010).
1137 15. Vitart, V. *et al.* New loci associated with central cornea thickness include COL5A1,
1138 AKAP13 and AVGR8. *Hum. Mol. Genet.* **19**, 4304–4311 (2010).

1139 16. Hoehn, R. *et al.* Population-based meta-analysis in Caucasians confirms association with
1140 COL5A1 and ZNF469 but not COL8A2 with central corneal thickness. *Hum. Genet.* **131**, 1783–
1141 1793 (2012).
1142 17. Gao, X. *et al.* A genome-wide association study of central corneal thickness in Latinos.
1143 *Invest. Ophthalmol. Vis. Sci.* **54**, 2435–2443 (2013).
1144 18. Iglesias, A. I. *et al.* Cross-ancestry genome-wide association analysis of corneal thickness
1145 strengthens link between complex and Mendelian eye diseases. *Nat. Commun.* **9**, 1864 (2018).
1146 19. Gao, X. *et al.* Genome-wide association study identifies WNT7B as a novel locus for
1147 central corneal thickness in Latinos. *Hum. Mol. Genet.* **25**, 5035–5045 (2016).
1148 20. Fan, B. J. *et al.* Family-Based Genome-Wide Association Study of South Indian Pedigrees
1149 Supports WNT7B as a Central Corneal Thickness Locus. *Invest. Ophthalmol. Vis. Sci.* **59**, 2495–
1150 2502 (2018).
1151 21. Ivarsdottir, E. V. *et al.* Sequence variation at ANAPC1 accounts for 24% of the variability
1152 in corneal endothelial cell density. *Nat. Commun.* **10**, 1284 (2019).
1153 22. Simcoe, M. J., Khawaja, A. P., Hysi, P. G., Hammond, C. J. & UK Biobank Eye and Vision
1154 Consortium. Genome-wide association study of corneal biomechanical properties identifies over
1155 200 loci providing insight into the genetic etiology of ocular diseases. *Hum. Mol. Genet.* **29**, 3154–
1156 3164 (2020).
1157 23. Han, X. *et al.* Automated AI labeling of optic nerve head enables insights into cross-
1158 ancestry glaucoma risk and genetic discovery in >280,000 images from UKB and CLSA. *Am. J.*
1159 *Hum. Genet.* **108**, 1204–1216 (2021).
1160 24. Yan, W. *et al.* Cell Atlas of The Human Fovea and Peripheral Retina. *Sci. Rep.* **10**, 9802
1161 (2020).
1162 25. Dharmat, R., Kim, S., Li, Y. & Chen, R. Single-Cell Capture, RNA-seq, and Transcriptome
1163 Analysis from the Neural Retina. *Methods Mol. Biol.* **2092**, 159–186 (2020).
1164 26. van Zyl, T. *et al.* Cell atlas of aqueous humor outflow pathways in eyes of humans and
1165 four model species provides insight into glaucoma pathogenesis. *Proc. Natl. Acad. Sci. U. S. A.*
1166 **117**, 10339–10349 (2020).
1167 27. Patel, G. *et al.* Molecular taxonomy of human ocular outflow tissues defined by single-cell
1168 transcriptomics. *Proc. Natl. Acad. Sci. U. S. A.* **117**, 12856–12867 (2020).
1169 28. van Zyl Wenjun Yan Alexi McAdams Aboozar Monavarfeshani Gregory S. Hageman
1170 Joshua R. Sanes, T. Cell atlas of the human ocular anterior segment: Tissue-specific and shared
1171 cell types. *bioRxiv* (2022) doi:10.1101/2022.01.19.476971.

1172 29. GTEx Consortium. The GTEx Consortium atlas of genetic regulatory effects across
1173 human tissues. *Science* **369**, 1318–1330 (2020).
1174 30. Gamazon, E. R. *et al.* Using an atlas of gene regulation across 44 human tissues to
1175 inform complex disease- and trait-associated variation. *Nat. Genet.* **50**, 956–967 (2018).
1176 31. Finucane, H. K. *et al.* Heritability enrichment of specifically expressed genes identifies
1177 disease-relevant tissues and cell types. *Nat. Genet.* **50**, 621–629 (2018).
1178 32. Ratnapriya, R. *et al.* Retinal transcriptome and eQTL analyses identify genes associated
1179 with age-related macular degeneration. *Nat. Genet.* **51**, 606–610 (2019).
1180 33. Strunz, T. *et al.* A mega-analysis of expression quantitative trait loci in retinal tissue. *PLoS*
1181 *Genet.* **16**, e1008934 (2020).
1182 34. Hormozdiari, F. *et al.* Colocalization of GWAS and eQTL Signals Detects Target Genes.
1183 *Am. J. Hum. Genet.* **99**, 1245–1260 (2016).
1184 35. Wen, X., Pique-Regi, R. & Luca, F. Integrating molecular QTL data into genome-wide
1185 genetic association analysis: Probabilistic assessment of enrichment and colocalization. *PLoS*
1186 *Genet.* **13**, e1006646 (2017).
1187 36. Eraslan, G. *et al.* Single-nucleus cross-tissue molecular reference maps to decipher
1188 disease gene function. *bioRxiv* 2021.07.19.452954 (2021) doi:10.1101/2021.07.19.452954.
1189 37. Rouhana, J., J. Wang, G. Eraslan, S. Anand, A. Hamel, B. Cole, A. Regev, F. Aguet, K.
1190 Ardlie, and A. V. Segrè. ECLIPSER: identifying causal cell types and genes for complex traits
1191 through single cell enrichment of e/sQTL-mapped genes in GWAS loci. *BioRxiv* (2021)
1192 doi:10.1101/2021.11.24.469720.
1193 38. Barbeira, A. N. *et al.* Exploiting the GTEx resources to decipher the mechanisms at
1194 GWAS loci. *Genome Biol.* **22**, 49 (2021).
1195 39. Wiggs, J. L. *et al.* Common variants at 9p21 and 8q22 are associated with increased
1196 susceptibility to optic nerve degeneration in glaucoma. *PLoS Genet.* **8**, e1002654 (2012).
1197 40. Collantes, E. R. A. *et al.* EFEMP1 rare variants cause familial juvenile-onset open-angle
1198 glaucoma. *Hum. Mutat.* **43**, 240–252 (2022).
1199 41. van Zyl Gregory Hagemna Joshua R. Sanes, A. M. W. Y. T. Cell atlas of the human optic
1200 nerve and optic nerve head. *bioRxiv (in preparation)* (2022).
1201 42. Lewczuk, K., Jabłońska, J., Konopińska, J., Mariak, Z. & Rękas, M. Schlemm's canal: the
1202 outflow 'vessel'. *Acta Ophthalmol.* (2021) doi:10.1111/aos.15027.
1203 43. GTEx Consortium *et al.* Genetic effects on gene expression across human tissues. *Nature*
1204 **550**, 204–213 (2017).

1205 44. Claussnitzer, M. *et al.* FTO Obesity Variant Circuitry and Adipocyte Browning in Humans.
1206 *N. Engl. J. Med.* **373**, 895–907 (2015).
1207 45. Nasser, J. *et al.* Genome-wide enhancer maps link risk variants to disease genes. *Nature*
1208 **593**, 238–243 (2021).
1209 46. Cao, J. *et al.* Joint profiling of chromatin accessibility and gene expression in thousands of
1210 single cells. *Science* **361**, 1380–1385 (2018).
1211 47. Mackay, D. S., Bennett, T. M. & Shiels, A. Exome Sequencing Identifies a Missense
1212 Variant in EFEMP1 Co-Segregating in a Family with Autosomal Dominant Primary Open-Angle
1213 Glaucoma. *PLoS One* **10**, e0132529 (2015).
1214 48. Lim, S.-H. *et al.* CYP1B1, MYOC, and LTBP2 mutations in primary congenital glaucoma
1215 patients in the United States. *Am. J. Ophthalmol.* **155**, 508–517.e5 (2013).
1216 49. Fuchshofer, R. & Tamm, E. R. The role of TGF-β in the pathogenesis of primary open-
1217 angle glaucoma. *Cell Tissue Res.* **347**, 279–290 (2012).
1218 50. Scerbo, P. & Monsoro-Burq, A. H. The vertebrate-specific VENTX/NANOG gene
1219 empowers neural crest with ectomesenchyme potential. *Sci Adv* **6**, eaaz1469 (2020).
1220 51. Kumar, S., Kumar, V., Li, W. & Kim, J. Ventx Family and Its Functional Similarities with
1221 Nanog: Involvement in Embryonic Development and Cancer Progression. *Int. J. Mol. Sci.* **23**,
1222 (2022).
1223 52. Fadini, G. P. *et al.* Reduced endothelial progenitor cells and brachial artery flow-mediated
1224 dilation as evidence of endothelial dysfunction in ocular hypertension and primary open-angle
1225 glaucoma. *Acta Ophthalmol.* **88**, 135–141 (2010).
1226 53. Su, W.-W. *et al.* Glaucoma is associated with peripheral vascular endothelial dysfunction.
1227 *Ophthalmology* **115**, 1173–1178.e1 (2008).
1228 54. Green, K. J., Getsios, S., Troyanovsky, S. & Godsel, L. M. Intercellular junction assembly,
1229 dynamics, and homeostasis. *Cold Spring Harb. Perspect. Biol.* **2**, a000125 (2010).
1230 55. Pattabiraman, P. P., Epstein, D. L. & Rao, P. V. Regulation of Adherens Junctions in
1231 Trabecular Meshwork Cells by Rac GTPase and their influence on Intraocular Pressure. *J. Ocul.*
1232 *Biol. Dis. Infor.* **1**, (2013).
1233 56. Gould, D. B., Smith, R. S. & John, S. W. M. Anterior segment development relevant to
1234 glaucoma. *Int. J. Dev. Biol.* **48**, 1015–1029 (2004).
1235 57. Pasquale, L. R. *et al.* CDKN2B-AS1 genotype-glaucoma feature correlations in primary
1236 open-angle glaucoma patients from the United States. *Am. J. Ophthalmol.* **155**, 342–353.e5
1237 (2013).

1238 58. Wang, H. *et al.* Physiological function of myocilin and its role in the pathogenesis of
1239 glaucoma in the trabecular meshwork (Review). *Int. J. Mol. Med.* **43**, 671–681 (2019).
1240 59. Hukku, A. *et al.* Probabilistic colocalization of genetic variants from complex and
1241 molecular traits: promise and limitations. *Am. J. Hum. Genet.* **108**, 25–35 (2021).
1242 60. Wallace, C. Eliciting priors and relaxing the single causal variant assumption in
1243 colocalisation analyses. *PLoS Genet.* **16**, e1008720 (2020).
1244 61. Zhu, Z. *et al.* Integration of summary data from GWAS and eQTL studies predicts complex
1245 trait gene targets. *Nat. Genet.* **48**, 481–487 (2016).
1246 62. Hemani, G., Bowden, J. & Davey Smith, G. Evaluating the potential role of pleiotropy in
1247 Mendelian randomization studies. *Hum. Mol. Genet.* **27**, R195–R208 (2018).
1248 63. Finucane, H. K. *et al.* Partitioning heritability by functional annotation using genome-wide
1249 association summary statistics. *Nat. Genet.* **47**, 1228–1235 (2015).
1250 64. Watanabe, K., Taskesen, E., van Bochoven, A. & Posthuma, D. Functional mapping and
1251 annotation of genetic associations with FUMA. *Nat. Commun.* **8**, 1826 (2017).
1252 65. Jagadeesh, K. A. *et al.* Identifying disease-critical cell types and cellular processes across
1253 the human body by integration of single-cell profiles and human genetics. *bioRxiv*
1254 2021.03.19.436212 (2021) doi:10.1101/2021.03.19.436212.
1255 66. Slowikowski, K., Hu, X. & Raychaudhuri, S. SNPsea: an algorithm to identify cell types,
1256 tissues and pathways affected by risk loci. *Bioinformatics* **30**, 2496–2497 (2014).
1257 67. Calderon, D. *et al.* Inferring Relevant Cell Types for Complex Traits by Using Single-Cell
1258 Gene Expression. *Am. J. Hum. Genet.* **101**, 686–699 (2017).
1259 68. Stamer, W. D. & Acott, T. S. Current understanding of conventional outflow dysfunction in
1260 glaucoma. *Curr. Opin. Ophthalmol.* **23**, 135–143 (2012).
1261 69. Goel, M., Picciani, R. G., Lee, R. K. & Bhattacharya, S. K. Aqueous humor dynamics: a
1262 review. *Open Ophthalmol. J.* **4**, 52–59 (2010).
1263 70. Alarcon-Martinez, L. *et al.* Pericyte dysfunction and loss of interpericyte tunneling
1264 nanotubes promote neurovascular deficits in glaucoma. *Proc. Natl. Acad. Sci. U. S. A.* **119**,
1265 (2022).
1266 71. Wang, R., Seifert, P. & Jakobs, T. C. Astrocytes in the Optic Nerve Head of
1267 Glaucomatous Mice Display a Characteristic Reactive Phenotype. *Invest. Ophthalmol. Vis. Sci.*
1268 **58**, 924–932 (2017).
1269 72. Zhao, X., Sun, R., Luo, X., Wang, F. & Sun, X. The Interaction Between Microglia and
1270 Macroglia in Glaucoma. *Front. Neurosci.* **15**, 610788 (2021).

1271 73. Shinozaki, Y. & Koizumi, S. Potential roles of astrocytes and Müller cells in the
1272 pathogenesis of glaucoma. *J. Pharmacol. Sci.* **145**, 262–267 (2021).
1273 74. Tovar-Vidales, T., Wordinger, R. J. & Clark, A. F. Identification and localization of lamina
1274 cribrosa cells in the human optic nerve head. *Exp. Eye Res.* **147**, 94–97 (2016).
1275 75. Lopez, N. N., Clark, A. F. & Tovar-Vidales, T. Isolation and characterization of human
1276 optic nerve head astrocytes and lamina cribrosa cells. *Exp. Eye Res.* **197**, 108103 (2020).
1277 76. Tamm, E. R., Ethier, C. R. & Lasker/IRRF Initiative on Astrocytes and Glaucomatous
1278 Neurodegeneration Participants. Biological aspects of axonal damage in glaucoma: A brief
1279 review. *Exp. Eye Res.* **157**, 5–12 (2017).
1280 77. Paula, J. S., O'Brien, C. & Stamer, W. D. Life under pressure: The role of ocular cribriform
1281 cells in preventing glaucoma. *Exp. Eye Res.* **151**, 150–159 (2016).
1282 78. Venkataraman, S. T., Flanagan, J. G. & Hudson, C. Vascular reactivity of optic nerve
1283 head and retinal blood vessels in glaucoma--a review. *Microcirculation* **17**, 568–581 (2010).
1284 79. Zeng, H.-L. & Shi, J.-M. The role of microglia in the progression of glaucomatous
1285 neurodegeneration- a review. *Int. J. Ophthalmol.* **11**, 143–149 (2018).
1286 80. Kim-Hellmuth, S., Aguet, F. & Oliva, M. Cell type–specific genetic regulation of gene
1287 expression across human tissues. (2020).
1288 81. van der Wijst, M. *et al.* The single-cell eQTLGen consortium. *Elife* **9**, (2020).
1289 82. Li, Y. I. *et al.* Annotation-free quantification of RNA splicing using LeafCutter. *Nat. Genet.*
1290 **50**, 151–158 (2018).
1291 83. Pruim, R. J. *et al.* LocusZoom: regional visualization of genome-wide association scan
1292 results. *Bioinformatics* **26**, 2336–2337 (2010).
1293 84. Zheng-Bradley, X. *et al.* Alignment of 1000 Genomes Project reads to reference assembly
1294 GRCh38. *Gigascience* **6**, 1–8 (2017).
1295 85. Pividori, M. *et al.* PhenomeXcan: Mapping the genome to the phenome through the
1296 transcriptome. doi:10.1101/833210.
1297 86. Brown, A. A. *et al.* Predicting causal variants affecting expression by using whole-genome
1298 sequencing and RNA-seq from multiple human tissues. *Nat. Genet.* **49**, 1747–1751 (2017).
1299 87. Finak, G. *et al.* MAST: a flexible statistical framework for assessing transcriptional
1300 changes and characterizing heterogeneity in single-cell RNA sequencing data. *Genome Biol.* **16**,
1301 278 (2015).
1302 88. Lakkis, J. *et al.* A joint deep learning model enables simultaneous batch effect correction,
1303 denoising, and clustering in single-cell transcriptomics. *Genome Res.* **31**, 1753–1766 (2021).

1304 89. Ghoussaini, M. *et al.* Open Targets Genetics: systematic identification of trait-associated
1305 genes using large-scale genetics and functional genomics. *Nucleic Acids Res.* **49**, D1311–D1320
1306 (2021).
1307 90. Storey, J. D. & Tibshirani, R. Statistical significance for genomewide studies. *Proc. Natl.*
1308 *Acad. Sci. U. S. A.* **100**, 9440–9445 (2003).
1309 91. Gamazon, E. R., Huang, R. S., Dolan, M. E., Cox, N. J. & Im, H. K. Integrative genomics:
1310 quantifying significance of phenotype-genotype relationships from multiple sources of high-
1311 throughput data. *Front. Genet.* **3**, 202 (2012).
1312 92. Pollack, S. *et al.* Multiethnic Genome-Wide Association Study of Diabetic Retinopathy
1313 Using Liability Threshold Modeling of Duration of Diabetes and Glycemic Control. *Diabetes* **68**,
1314 441–456 (2019).
1315 93. Li, B. & Dewey, C. N. RSEM: accurate transcript quantification from RNA-Seq data with or
1316 without a reference genome. *BMC Bioinformatics* vol. 12 (2011).